Obox4 promotes zygotic genome activation upon loss of *Dux*

Youjia Guo[#1], Tomohiro Kitano[#1], Kimiko Inoue[#2,3], Kensaku Murano[1], Michiko Hirose[2], Ten D. Li[1], Akihiko Sakashita[1], Hirotsugu Ishizu[1], Narumi Ogonuki[2,3], Shogo Matoba[2,3], Masayuki Sato[1], Atsuo Ogura[*2,3], Haruhiko Siomi[*1]

[1]Department of Molecular Biology, Keio University School of Medicine, Shinjuku, Tokyo 160-8582, Japan;
[2]Human Biology Microbiome Quantum Research Center (WPI-Bio2Q), Keio University, Shinjuku, Tokyo 160-8582, Japan;
[3]Bioresource Engineering Division, Bioresource Center, RIKEN, Tsukuba, Ibaraki 305-0074, Japan;
[4]Graduate School of Life and Environmental Sciences, University of Tsukuba, Tsukuba, Ibaraki 305-8577, Japan

[#]These authors contributed equally: Youjia Guo, Tomohiro Kitano, and Kimiko Inoue.

[*]Corresponding author:
Haruhiko Siomi awa403@keio.jp
Atsuo Ogura ogura@rtc.riken.go.jp

Abstract

Once fertilized, mouse zygotes rapidly proceed to zygotic genome activation (ZGA), during which long terminal repeats (LTRs) of murine endogenous retroviruses with leucine tRNA primer (MERVL) are activated by a conserved homeodomain-containing transcription factor, DUX. However, *Dux*-knockout embryos produce fertile mice, suggesting that ZGA is redundantly driven by an unknown factor(s). Here we present multiple lines of evidence that the multicopy homeobox gene, *Obox4*, encodes a transcription factor that is highly expressed in mouse 2-cell embryos and redundantly drives ZGA. Genome-wide profiling revealed that OBOX4 specifically binds and activates MERVL LTRs as well as a subset of murine endogenous retroviruses with lysine tRNA primer (MERVK) LTRs. Depletion of *Obox4* is tolerated by embryogenesis, whereas concomitant *Obox4/Dux* depletion markedly compromises embryonic development. Our study identified OBOX4 as a transcription factor that provides genetic redundancy to pre-implantation development.

Introduction

The mechanism by which zygotes acquire totipotency is a major question in Developmental Biology. Following fertilization, the zygote must build a *de novo* conceptus with a transcriptionally quiescent genome. The genome rapidly undergoes zygotic genome activation (ZGA), during which epigenetic reprogramming and expression of nascent transcripts enforce the replacement of parental infrastructures by their zygotic counterparts [1]. Completion of metazoan ZGA results in blastomeres, a collection of cells that are totipotent enough to reflect their potential to individually produce both embryos and extraembryonic appendages [2,3]. Totipotency lasts until the morula stage, where the first cell

fate decision takes place, following which it is remolded into pluripotency in cells destined for the embryonic lineage [4], to which embryonic stem cells (ESCs) and induced pluripotent stem cells (iPSCs) correspond. In placental mammals, ZGA is characterized by the massive reactivation of transposable elements (TEs) and epigenome remodeling, predominantly implemented by a collection of ZGA genes that have adapted long terminal repeats (LTRs) of endogenous retroviruses (ERVs) as stage-specific *cis*-regulatory elements [5].

Homeodomains are DNA-binding amino acid motifs encoded by a class of conserved genomic sequences termed homeoboxes [6-8]. Homeodomains are prevalent transcription factors that regulate development because of their ability to bind chromatin in a sequence-specific manner [9-11]. Among all homeobox-containing genes, Paired-like (PRD-like) homeobox class genes are particularly associated with ZGA [12]. Studies have shown that the PRD-like homeobox gene, double homeobox (*Dux*), plays an important role in pre-implantation embryogenesis [13,14]. *Dux* is conserved throughout placentalia and is highly expressed during ZGA. In humans and mice, DUX specifically binds and activates endogenous retroviruses with leucine tRNA primer (ERVL) LTR-derived promoters, resulting in the expression of downstream ZGA genes [15-17]. *Dux* expression induces a 2-cell-embryo-like (2C-like) state in mouse embryonic stem cells (mESCs) [15-17], whereas *Dux*-knockout (KO) undermines mouse blastocyst formation [15]. However, subsequent studies have revealed that mouse embryogenesis is compatible with the loss of *Dux*, suggesting a redundant pathway of ZGA that is controlled by uncharacterized transcription factor(s) [18-21].

In this study, we sought to identify the redundant transcription factor that drives ZGA in the absence of *Dux*. We discovered that the multicopy homeobox gene, oocyte-specific homeobox 4 (*Obox4*), promotes *Dux*-less ZGA. *Obox4* is abundantly expressed in mouse 2C-embryos, 2C-like mESCs, and totipotent blastomere-like cells (TBLCs) [22]. Mechanistically, OBOX4 promotes ZGA by binding to the LTRs of murine endogenous retroviruses with leucine tRNA primer (MERVL) and murine endogenous retroviruses with lysine tRNA primer (MERVK), and thereby affecting the deposition of active epigenetic modifications. Concomitant, but not respective, depletion of *Obox4* and *Dux* severely compromises ZGA and preimplantation development. Taken together, our findings substantiate a pre-implantation development model, in which the ZGA is redundantly promoted by *Dux* and *Obox4*.

Results

Expression profiling identifies transcription factor candidates

Genetic redundancy is commonly observed among genes that share sequence homology [23]. Because *Dux* is a homeobox gene, we speculated that its redundant factors are homeobox genes. We examined the expression profiles of all mouse homeobox genes during pre-implantation embryogenesis using published single-cell RNA-seq (scRNA-seq) data [24]. Clustering analysis defined a collection of 45 homeobox genes, whose transcript levels reached a maximum before the late 2C stage (Fig. 1a). We then sought to identify *bona fide* ZGA factors from this collection by looking for genes whose transcripts were of zygotic origin, instead of ones that were parentally inherited. TBLCs have recently been established *as in vitro* counterparts of 2C-embryos, which are derived from splicing-inhibited mESCs, and hence, are free of parentally inherited transcripts [22]. Analysis of published RNA sequencing (RNA-seq) data showed that the expression of four homeobox genes, *Duxf3*, *Emx2*, *Hoxd13*, and *Obox4*, was ten times higher in TBLCs than in ESCs (Fig. 1b). We examined whether the expression of these genes was affected in the *Dux* knockout embryos. Using

published RNA-seq data [18,20], we found that the expression of all single-copy candidate genes and a subset of the multicopy gene *Obox4* was unaffected in *Dux* knockout embryos (Fig. 1c).

Obox4 **activates 2C-genes and TEs in mESC**

Before examining whether the candidates were crucial for embryogenesis, we first confirmed the presence of endogenous OBOX4 protein, as the *Obox4* loci are marked as pseudogenes in the current genome annotation GRCm39 [25]. We generated mouse anti-OBOX4 monoclonal antibodies. Immunofluorescence staining using these antibodies confirmed that endogenous OBOX4 was expressed in zygotes and highly abundant in 2C-embryos and 2C-like mESCs (Fig. 1d-e), which is consistent with translatome profile captured by Ribo-seq that detects OBOX4 translation at 2C stage [26] (Fig. 1f). Mouse ZGA is characterized by the surging activity of genes that specifically express at 2C stage (2C-gene), many of which have co-opted MERVL LTRs as stage-specific promoters [27]. We then sought to examined whether the candidates had potential to promote ZGA by activating MERVL and 2C-genes (Supplementary Fig. 1a and Supplementary Table 1-2). We constructed a 2C::tdTomato reporter mESC line with transgenic tdTomato red fluorescence protein driven by MERVL 5'-LTR. [28] (Fig. 2a). Candidate genes were cloned and overexpressed in the reporter cell line (Supplementary Fig. 1b-c). Interestingly, ectopic expression of *Obox4* markedly induced tdTomato expression, similar to that induced by *Dux* (Fig. 2b and Supplementary Fig. 2a-b). To characterize the impact of *Obox4* expression on 2C-genes, we established an ESC stable line bearing an inducible *Obox4* transgene (Fig. 2c). Differentially expressed gene analysis revealed that *Obox4* induction led to transcriptome changes in mESCs, characterized by upregulation of 2C-genes and TEs that were highly expressed in early-to-middle 2C-embryos [29] (Fig. 2d-e), naturally occurred 2C-like mESCs [30], and *Dux* induced 2C-like mESCs [16] (Fig. 2f, Supplementary Table 3). A substantial fraction (159/164) of *Obox4* induced 2C genes were also induced by *Dux* (Fig. 2g), while transcriptomic perturbance induced by *Obox4* is milder comparing with *Dux*, characterized by less number and less fold-upregulation of 2C genes (Fig. 2g-h). Interestingly, Dux and Obox4 were mutually inductive, where one promoted expression of the other (Fig. 2h). These results suggest that *Obox4* is an inducer of 2C-like genes and potentially redundant factor of *Dux*.

Obox4 binds to 2C-gene promoters and LTR elements in mESC

Obox4 contains a homeobox, activates 2C-genes and TEs, and upregulates *Dux*-induced genes, which prompted us to examine whether OBOX4 is a transcription factor that activates 2C-gene associated loci through direct binding with *cis*-regulatory elements. Cleavage under targets and release using nuclease (CUT&RUN) leverages antibody-targeted cleavage of proximal DNA to identify the binding sites of DNA-associated proteins [31]. To examine this technique, we performed CUT&RUN against triple FLAG-tagged DUX (3×FLAG-DUX) expressed in mESCs using a high-affinity anti-FLAG antibody [32], and confirmed that the DUX binding pattern revealed by CUT&RUN recapitulated the published HA-tagged DUX ChIP data [16] (Supplementary Fig. 3a-b). We then proceeded with characterizing genomic footprint of OBOX4 by performing CUT&RUN against 3×FLAG-OBOX4 expressed in mESCs, and discovered ~24,000 peaks, among which 39.5% located in the gene promoter regions that covered 26.8% (273/1,019) of the 2C-genes (Fig. 3a). *De novo* motif discovery using the top 500 CUT&RUN signal peaks predicted CTGGGATYWRMR as top OBOX4 binding motif, which is enriched in the promoter regions of 2C-genes (Fig. 3b). Collectively, OBOX4 and DUX targeted 48.1% (490/1,019) of the 2C-genes with a considerable overlap (36.3% for OBOX4 and 31.3% for DUX), which covered many important ZGA genes including *Dppa2*, *Sp110*, and *Zscan4d* (Fig. 3c-d and Supplementary

Table 4). The overlap was substantiated by the observation that MERVL LTR MT2_Mm was among the top 10 LTR targets of both OBOX4 and DUX, based on loci coverage (Fig. 3e-f and Supplementary Table 5). Notably, while DUX strongly prefers MT2_Mm, OBOX4 binding was biased toward MERVK LTRs, namely RLTR9 and RLTR13 elements (Fig. 3g), which also demonstrated a 2C-specific expression profile (Supplementary Fig. 3c-d). To examine whether these bindings were functional in the absence of *Dux*, we generated Obox4/Dux single and double knockout mECS lines, in which 14 of 15 protein-coding *Obox4* copies were removed from the genome (Supplementary Fig. 4-5). tdTomato reporters driven by MT2_Mm and RLTR13B2 were co-transfected with *Dux* and *Obox4* into *Obox4/Dux* double knockout ESCs (Fig. 3h). Analysis of the tdTomato-positive population showed that *Obox4* activated both RLTR13B2 and MT2_Mm, whereas *Dux* only activated MT2_Mm (Fig. 3i). These observations demonstrated that OBOX4 binds and activates a subset of DUX targets in mESCs and redundantly drives their expression in the absence of DUX.

Concomitant loss of *Obox4* and *Dux* impairs preimplantation development

We then sought to determine whether *Obox4* is functionally required for pre-implantation development, particularly in the absence of *Dux*. Transient depletion of DUX has previously confused the field in that it caused an embryonic phototype while subsequent *Dux* knockout females were shown to be fertile [15,18-21]. Therefore, it is critical to examine the functional requirement of OBOX4 and DUX in genetic knockout models. Somatic cell nuclear transfer (SCNT) is a technique to create embryos by transferring nuclei of somatic cells into enucleated oocytes (Fig. 4a), which recapitulates ZGA [33]. When the knockout mESCs were subjected to SCNT as nuclear donors, 54.4% of WT mESC derived embryos developed to blastocyst stage at 4 days post nuclear transfer (dpt). *Obox4* and *Dux* single knockout donors led to reduced blastocyst formation rate at 38.5% and 39.7% respectively, whereas double knockout resulted in additive effect that led to significantly lowered blastocyst rate of 29.3% (Fig. 4b). Notably, all the blastocysts derived from double knockout mESC were of low quality, judging from severe morphological abnormality (Fig. 4c).

As an alternative genetic knockout model, we generated mice bearing *Dux* and *Obox4* knockout allele by direct CRISPR-Cas9 editing in embryos (Fig. 4d and Supplementary Fig. 4a-b). Among 39 *Obox4* copies, there are 15 copies that maintain intact open reading frame (ORF) for full-length OBOX4 (Supplementary Fig. 4c). While 14 of the 15 intact ORFs form tightly packed cluster (*Obox4* cluster), a solo ORF (*Obox4-ps33*) remains distant from the *Obox4* cluster and is interspersed with *Obox1/2/3*, a collection of *Obox* family members that are critical for ZGA [34]. To minimize collateral genetic toxicity and interference to experiment result caused by removal of other *Obox* members, only *Obox4* cluster was knocked out and the solo ORF was retained (Supplementary Fig. 4d and Supplementary Fig. 6). The observed $Obox4^{KO}$ frequency (7/29) in the progenies of $Obox4^{Het} \times Obox4^{Het}$ crossing is consistent with the expected 25% Mendelian ratio (Fig. 4e, Supplementary Fig. 7, and Supplementary Table 6). That $Obox4^{KO}$ mice developed to adulthood without discernable abnormalities and are fertile when intercrossed suggest that development is compatible with loss of *Obox4* (Fig. 4f-g). We next attempted to produce *Dux/Obox4* double knockout ($Dux^{KO}/Obox4^{KO}$) mice to examine whether concomitant loss of *Dux* and *Obox4* compromises embryogenesis. We genotyped 54 pups from three litters of $Dux^{KO}/Obox4^{Het} \times Dux^{KO}/Obox4^{Het}$ and six litters of $Dux^{KO}/Obox4^{Het} \times Dux^{Het}/Obox4^{Het}$ mating pairs (Supplementary Fig. 8 and Supplementary Table 6). One $Obox4^{KO}/Dux^{KO}$ pup was present, and the frequency of $Obox4^{KO}/Dux^{KO}$ and $Obox4^{KO}/Dux^{Het}$ were significantly lower than the expected 25% Mendelian ratio (Fig. 4h). Development monitoring and genotyping of embryos produced by $Dux^{KO}/Obox4^{Het} \times Dux^{Het}/Obox4^{Het}$ mating pairs at

4.5 days post cotium (dpc) revealed that *Dux*^{KO}/*Obox4*^{KO} was under-represented in blastocysts while over-represented in 2-cell arrest and degenerated embryos (Fig. 4i, Supplementary Fig. 9a-c, and Supplementary Table 7). Single blastomere genotyping and RNA-seq of *Dux*^{KO}/*Obox4*^{KO} 2C embryos (Supplementary Fig. 9d-e) showed dysregulation of 2C-genes and TEs targeted by OBOX4 (Fig. 4j). The impaired development and transcriptome of *Dux*^{KO}/*Obox4*^{KO} embryos at 2-cell stage showed that ZGA was defective in those embryos.

As a transient depletion model in addition to genetic knockout approaches, microinjection of antisense oligonucleotide (ASO) into male pronuclei of zygotes was performed to knockdown *Obox4* and *Dux* (Fig. 4k and Supplementary Fig. 10a-c). Monitoring development until 4.5 dpc showed that *Obox4* single knockdown resulted in moderate developmental retardation, with almost 50% of embryos reaching the blastocyst stage. Similarly, blastocyst formation was preserved in nearly 25% of *Dux* single knockdown embryos, which is consistent with previously reported *Dux* knockdown/knockout experiments [15,18-21]. The *Obox4*/*Dux* double knockdown markedly compromised blastocyst formation, resulted in more than 80% embryos degenerated or arrested before the 4C stage, and less than 20% manifested morula-like morphology (Fig. 4k-l). The double knockdown embryos with morula-like morphology manifest dysregulated transcriptome characterized by failure of expressing morula specific genes and activation of apoptosis related pathways, suggesting that the development was dysfunctional instead of delayed (Supplementary Fig. 10e-g).

The consistency among constitutive knockout in SCNT embryos and living mice and ASO-mediated transient depletion demonstrated that the expression of *Obox4* and *Dux* is collectively important for pre-implantation development, and that *Obox4* is capable of promoting ZGA in a *Dux*-independent manner. Collectively, these data show that *Obox4* promotes mouse preimplantation development in the absence of *Dux*.

OBOX4 promotes 2C-gene expression upon depletion of DUX

As *Obox4* has been shown to activate 2C-genes and TEs in mESCs, and embryonic depletion of OBOX4 impairs 2C-genes and TEs activation, we questioned whether the impairment can be ameliorated by restoration of OBOX4. First, we determined whether the presence of OBOX4 can rescue the developmental arrest of *Obox4*/*Dux* double knockdown embryos. Codon-optimized *Obox4* mRNA without the ASO target motif was produced using *in vitro* transcription. The rescue experiment was performed by means of co-microinjection of *Obox4* mRNA with *Obox4*/*Dux* double knockdown ASOs (Fig. 5a). Restoration of OBOX4 in *Obox4* mRNA-microinjected embryos was confirmed using immunofluorescence staining at the 2C stage (Fig. 5b). As expected, development monitoring showed that *Obox4*/*Dux* double knockdown embryos failed blastocyst formation at 4.5 dpc, whereas among *Obox4* mRNA-rescued embryos, blastocyst formation was retained at a similar level to that observed in the *Dux* single knockdown experiment (Fig. 5c-d and Fig. 4k-l). RNA-seq of 2C-embryos revealed exacerbated dysregulation of 2C-genes and TEs by *Obox4*/*Dux* double knockdown comparing to single knockdown, and the dysregulated transcriptome of double knockdown was rescued by resupplying OBOX4, revealed by number of up and down-regulated genes (Fig. 5e-f). Differential expression analysis revealed that 58% (102/175) of the down-regulated 2C-genes in double knockdown embryos were rescued, including 2C stage markers and important ZGA factors (Fig. 5g-h). These results showed that that OBOX4 redundantly activates 2C gene to promote ZGA under DUX depletion.

Discussion

Starting with a transcriptionally inert genome, the eutherian ZGA engages in massive yet coordinated expression of genes driven by LTR TEs. In mice, it has been reported that the transcription factor DUX accesses and opens condensed chromatin of the MERVL LTR loci, which results in the activation of downstream ZGA genes [15-17]. However, the establishment of fertile *Dux* knockout mice suggests that ZGA is redundantly driven by other transcription factor(s) [18-21]. In the present study, we found that *Obox4*, a cryptic multi-copy cluster gene, encodes a homeodomain-containing protein that potently induces ZGA gene expression. Using multiple genetic knockout models, we showed that concomitant depletion of *Dux* and *Obox4* was hardly compatible with embryogenesis, characterized by *Dux/Obox4* double knockout mESCs compromised SCNT and mouse produced at sub-Mendelian ratio. Consistently, *Obox4/Dux* double knockdown markedly compromised pre-implantation development, which tolerated single knockdown of either gene. Double knockdown embryos exhibited severely dysregulated transcriptomes, characterized by MERVL and ZGA gene activation failure. We also characterized the molecular mechanisms underlying the biological significance of *Obox4* as well as its relevance to *Dux*. OBOX4 directly binds to MERVL (the target of DUX) and MERVK loci and activates specific MERVL and MERVK elements in a *Dux*-independent manner. In summary, our results highlight that OBOX4 is a transcription factor that is functionally redundant to DUX during ZGA.

Obox transcripts were first discovered in gonads [35], and were later found to be highly abundant in mouse 2C-embryos [36]. The *Obox* family has 67 members clustered in the sub-telomeric region of mouse chromosome 7 and is further divided into six subfamilies: *Obox1*, *Obox2*, *Obox3*, *Obox4*, *Obox5*, and *Obox6*, with *Obox4* constituting nearly 60% (39 of 67) of the family population [37,38]. Although *Obox4* dominates the *Obox* family population, members of the entire subfamily have been annotated as pseudogenes and have largely been neglected from investigation. Despite being abundantly transcribed in the gonads, the biological significance of *Obox* genes is poorly understood. The role of *Obox4* is particularly mysterious, as it remains to be determined whether *Obox4* is a functional protein-coding gene. Transcription of *Obox4* was originally reported to be testis-specific and contradicted by the detection of *Obox4* transcripts in the ovaries and oocytes [39]. *Obox4* is involved in oocyte maturation and ESC differentiation [40-44]. However, these observations are supported by limited evidence, with no evidence at the protein level. By detecting OBOX4 in various totipotent cell types using high-quality monoclonal antibodies, we provided decisive evidence that *Obox4* is a functional protein-coding gene. Our data demonstrated that OBOX4 binds to genomic loci of MERVL-derived promoters and MERVK-derived enhancers and mediates their activation during ZGA. However, whether and how other *Obox* family members contribute to ZGA remains unclear.

It is worth noting that the ability of OBOX4 to promote ZGA appears to be weaker than that of DUX, characterized by lower fold upregulation of 2C-genes upon overexpression of OBOX4 than DUX, non-induction of MERVL Gag protein in mESCs, less dysregulated transcriptome in *Obox4* depleted embryos, and less adversarial phenotype in *Obox4* depleted embryos and mice. On the other hand, the severe cytotoxicity borne by DUX[45] cannot be observed in OBOX4, as ectopic expression of OBOX4 in mESCs and embryos did not show hindrance in cell viability. Whether the variance in potency to promote ZGA has additional biological significance other than functional redundancy warrants further investigation.

Unlike *Dux*, which is structurally and functionally conserved throughout placentalia [46], the ancestral locus of the *Obox* family appears to have undergone mouse-specific duplication and generated a gene cluster that is collectively

228 syntenic to the *Tprx2* locus in other mammals [47]. Despite the distal homology between *Obox4* and *Tprx2*, it has been
229 recently reported that human *TPRX2* is expressed in 8-cell embryos [14]. Interestingly, TPRX2 was shown to cause
230 defective ZGA upon embryonic depletion and bind important ZGA genes in hESCs [48], suggesting that the *Tprx2* locus
231 has undergone functionally convergent evolution despite its divergent genetic context. However, whether *TPRX2* plays
232 a similar role in humans to *Obox4* in mice regarding the redundancy to *Dux* (*DUX4* in humans) remains to be elucidated.
233 Genetic redundancy is widespread in higher organisms and typically arises in signaling networks, in which multiple
234 functionally overlapping factors commit to a shared teleological objective, to counteract sporadic mutations or defects
235 [49,50]. This principle is of particular importance to embryogenesis, a process that gives rise to a reproducing organism.
236 Indeed, genetic redundancy in pluripotency has been evidenced by the observation that naïve pluripotency can be
237 elicited and maintained through various "independent inputs that operate through both unique and convergent targets"
238 [51]. Although the molecular pathway that governs totipotency has been largely restricted to the scope that centers on
239 *Dux*, it is reasonable to assume that the acquisition of totipotency also complies with the rule of redundancy. This
240 assumption was validated by the generation of fertile *Dux* knockout mice; however, the panorama of ZGA redundancy
241 remained hidden. Our work on *Obox4* sheds light on this topic by discovering that *Obox4* serves as a redundant gene to
242 *Dux* during ZGA and is a bivalent activator of MERVL and MERVK elements. Yet that concomitant loss of *Dux* and
243 *Obox4* is viable reveals that ZGA is so strongly canalized that many differences in genes make very little difference to
244 the phenotype. Although the function of MERVL has been extensively investigated, particularly during early
245 embryogenesis, the role of MERVK remains unclear. Interestingly, recent studies have suggested that MERVK serves
246 as a meiosis-specific enhancer of spermatogenesis [52]. Mammalian Y chromosomes have undergone rapid evolution and
247 have been intensively inserted by TEs [53]. As *Obox4* is highly expressed in the testes, it is worth investigating whether
248 *Obox4* plays a regulatory role during spermatogenesis, by activating MERVK-derived enhancers.
249 Pioneer factors possess the ability to specifically recognize and access DNA motifs that are inaccessible to other
250 transcription factors [54]. In the scope of pluripotency-to-totipotency transition, OBOX4 and DUX are qualified pioneer
251 factors for they are capable of accessing and activating silenced 2C-genes in ESCs. However, it is not likely that such
252 pioneer activity demonstrated *in vitro* is accounted for ZGA initiation *in vivo*, considering that genome-wide
253 demethylation precedes the timing of OBOX4 and DUX translation [55], and neither individual nor collective depletion
254 of OBOX4 and DUX caused strict 2C arrest. Recent studies have identified the maternally deposited orphan nuclear
255 receptor NR5A2 that triggers ZGA by activating short interspersed nuclear element (SINE) B1 family [56,57], while DNA
256 damage induced p53 activation is important but dispensable for *Dux* activation in mouse zygotes [58]. These results suggest
257 another layer of genetic redundancy at ZGA initiation level. Hence, how *Dux* and *Obox4* are activated after fertilization
258 and whether they share the same activation mechanism requires further interrogation.
259

260 ## Figure Legends

261 **Figure 1. OBOX4 is expressed during ZGA.**

262 a) Mouse homeobox genes that are specifically expressed during ZGA. The genes were identified by means of
263 statistically determined *k*-means clustering based on their expression in pre-implantation embryos. *Dux* is shown
264 in a bold italic font.

265 b) Scatterplot showing per-gene normalized read counts in mouse totipotent TBLCs *versus* ESCs. Genes with more
266 than 10-fold normalized read counts (FC=10) have been highlighted. *Dux* is shown in a bold italic font.
267 c) MA plot displaying gene expression in *Dux* knockout 2C-embryos *versus* WT 2C-embryos. Loss of *Dux* partially
268 deactivates the multicopy homeobox gene *Obox4*.
269 d) Immunofluorescence staining of OBOX4 and MERVL GAG at different pre-implantation embryo stages.
270 e) Immunofluorescence staining of DUX, OBOX4, and OCT4 in 2C-like ESCs.
271 f) Translation profile of DUX and OBOX4 during preimplantation characterized by Ribo-seq signal.
272
273 **Figure 2. *Obox4* and *Dux* induce 2C-gene expression in mESCs.**
274 a) Diagram of the 2C::tdTomato reporter assay. ESCs bearing the tdTomato expression cassette under the control
275 of the MERVL LTR promoter showed red fluorescence upon entering the 2C-like state. The expression of the
276 transcription factor increased the 2C-like population, as detected using FACS. An EGFP expression plasmid was
277 co-transfected with a gene of interest, to normalize the transfection efficiency.
278 b) Boxplot showing normalized 2C-like cell percentage in 2C::tdTomato reporter ESCs overexpressing candidate
279 pioneer factors. *Dux* and *Obox4* potently induced a 2C-like state.
280 c) Upper panel: schematic of *Obox4*-inducible cell line construction. Lower panel: western blot showing OBOX4 level
281 upon induction by different concentrations of doxycycline. Expression of OBOX4 was carried out in a dose-
282 dependent manner.
283 d) Left panel: volcano plot of DEGs in mESCs with *Obox4* induction for 48 hours. Representative 2C-genes are
284 labeled with gene symbols. Right panel: expression profile of genes up-regulated by *Obox4* during embryogenesis.
285 e) Left panel: volcano plot of differentially expressed transposable elements in mESCs with *Obox4* induction for 48
286 hours. MERVL and MERVK elements were highlighted. Right panel: expression profile of MERVL and
287 MERVK elements during pre-implantation embryogenesis.
288 f) Heatmaps of the expression of 2C-genes in preimplantation embryos, naturally occurred 2C-like mESCs, and
289 induced 2C-like mESCs.
290 g) Venn diagram showing overlap of 2C-genes with genes induced by ectopic expression of *Dux* and *Obox4* in mESCs.
291 h) Scatterplot showing per-gene expression changes in *Dux* induced mESCs *versus Obox4* induced mESCs. 2C-genes
292 are highlighted in red. *Obox4* and *Dux* are labeled.
293
294 **Figure 3. OBOX4 binds and activates 2C-specific LTR elements.**
295 a) Left panel: pie-chart displaying proportions of annotated genomic regions of the OBOX4 binding sites. Right
296 panel: heatmap showing the OBOX4 binding site distribution near 2C-gene promoters.
297 b) Left panel: the predicted OBOX4 binding motif using the top 500 CUT&RUN peaks. Right panel: histograph
298 showing the distribution of predicted OBOX4 binding motif near 2C and random gene promoters.
299 c) Venn diagram showing the distinct and overlap 2C-genes targeted by DUX and OBOX4.
300 d) Representative genomic track showing DUX and OBOX4 binding sites at the *Dppa2*, *Sp110,* and *Zscan4d* loci and
301 their expression levels in *Obox4* and *Dux* induced mESCs. Read counts were CPM normalized. The OBOX4
302 binding sites overlapped with those of DUX. *Dppa2, Sp110*, and *Zscan4d* expression was upregulated upon *Obox4*
303 and *Dux* induction.

304 e) Left panel: pie-chart displaying proportions of annotated TEs of the OBOX4 binding sites. Right panel: Bar plot
305 showing the top 10 OBOX4 covered LTR elements.
306 f) Left panel: pie-chart displaying proportions of annotated TEs of the DUX binding sites. Right panel: Bar plot
307 showing the top 10 DUX covered LTR elements.
308 g) Representative genomic track showing DUX and OBOX4 binding sites at MT2_Mm and RLTR13B2. Read
309 counts were CPM normalized. The OBOX4 binding sites overlapped with those of DUX at MT2_Mm loci, while
310 RLTR13B2 was uniquely bound by OBOX4.
311 h) Schematic design of the LTR::tdTomato reporter assay. Plasmids bearing a tdTomato ORF downstream of
312 MT2_Mm or RLTR13B2 were co-transfected with *Dux* or *Obox4* expression plasmids. Activation of LTR elements
313 resulted in an increased red fluorescence-positive mESC population, which was measured using FACS. EGFP
314 expression plasmid was co-transfected into the culture, following which the green fluorescence-positive population
315 was measured, to normalize the transfection efficiency.
316 i) Bar plots showing the percentage of red fluorescence-positive mESCs upon expression of *Dux* or *Obox4*. Both *Dux*
317 and *Obox4* activated MT2_Mm, whereas only *Obox4* activated RLTR13B2.
318
319 **Figure 4. Concomitant loss of OBOX4 and DUX severely hinders ZGA.**
320 a) Schematic representation of somatic cell nuclear transfer (SCNT) experiment. The nuclei of knockout mESCs
321 were transferred to enucleated oocytes to generate zygotes with knockout genotype.
322 b) Upper panel: percent SCNT embryos developed to different stages at 4 dpt. Lower panel: *p*-value of non-
323 parametric analysis of variance (ANOVA) among different genotypes and stages comparing to wildtype SCNT
324 embryos. Three independent experiments were conducted, with 150-200 embryos per condition.
325 c) Representative picture of SCNT embryos at 4 dpt. Morphologically abnormal blastocysts are highlighted.
326 Blastocysts generated by double knockout mESCs were severely defective.
327 d) Schematic representation of CRISPR-Cas9 mediated *Dux* and *Obox4* knockout mouse production. *In vitro* fertilized
328 mouse zygotes were electroporated with pre-assembled CRISPR-Cas9 complex targeting *Dux* and *Obox4* loci.
329 e) Bar plot showing genotype percentage of the pups delivered by $Obox4^{Het}$ intercrosses. 4 litters delivered 29 pups,
330 litter size 7.25 ± 1.26. ns *p*-value = 0.9146, chi-square goodness of fit test.
331 f) Representative photos of $Obox4^{KO}$ and WT adult mice analyzed in **e**.
332 g) Photo of $Obox4^{KO}$ intercross litter with live pups.
333 h) Bar plot showing genotype of *Obox4* allele in the pups delivered by crossing of $Dux^{KO}/Obox4^{Het} \times Dux^{KO}/Obox4^{Het}$
334 or $Dux^{KO}/Obox4^{Het} \times Dux^{Het}/Obox4^{Het}$. Nine litters delivered 54 pups, *Dux* heterozygous and knockout allele were
335 present in 31 and 23 pups, respectively. ** *p*-value = 0.001306; * *p*-value = 0.02218; chi-square goodness of fit test.
336 i) Bar plot showing observed percentages of different preimplantation stage embryos bearing *Obox4* KO allele with
337 *Dux* heterozygous or knockout allele at 4.5 dpc. Among the total 94 embryos assessed, two degenerated, ten 2-cell
338 arrest, two 4-8 cell arrest, four morula arrest embryos were observed at 4.5 dpc, whereas 76 developed to blastocyst.
339 *** *p*-value = 3.564×10^{-5}; for 2-cell * *p*-value = 0.04348; for blastocyst * *p*-value = 0.02549; chi-square goodness
340 of fit test.

j) Scatterplot showing expression log2 fold changes of genes (left panel) and TEs (right panel) in *Dux*^{KO}/*Obox4*^{KO} *versus* *Dux*^{KO}/*Obox4*^{Het} 2C embryos. 2C-genes targeted by OBOX4 and ERVK elements are highlighted in blue. MT2_Mm and MERVL-int are labeled.

k) Upper panel: schematic representation of *Dux* and *Obox4* knockdown experiments in pre-implantation embryos. Male pronuclei of zygotes were microinjected with ASO targeting *Dux* or *Obox4* transcripts. Lower panel: the percentages of embryonic stages observed at 1.5 dpc, 2.5 dpc, 3.5 dpc, and 4.5 dpc.

l) Representative picture of KD embryos at 4.5 dpc. No blastocyst was observed among double ASO knockdown embryos.

Figure 5. OBOX4 promotes ZGA in the absence of DUX.

a) Schematic of the double knockdown rescue experiment. Male pronuclei of zygotes were injected with ASO targeting *Obox4* and *Dux* transcripts as well as *in vitro*-transcribed codon-optimized *Obox4* mRNA.

b) Immunofluorescence staining of OBOX4 in early 2-cell embryos microinjected with scrambled ASO, double ASO (*Obox4* and *Dux*), or double ASO with codon-optimized *Obox4* mRNA.

c) Representative picture of knockdown and rescue embryos at 4.5 dpc. Codon-optimized *Obox4* mRNA injection rescued blastocyst formation in ASO knockdown embryos.

d) The percentages of embryonic stages observed at 1.5 dpc, 2.5 dpc, 3.5 dpc, and 4.5 dpc. The plot represents the sum of three independent experiments, with 80-100 embryos per condition.

e) Upper panel: volcano plot showing the results of DEG analysis of 2C-genes in knockdown and rescue embryos, as compared to that in scramble ASO-injected embryos. Standard deviations of $\log_2$(fold-change) were used to represent the degree of transcriptome dysregulation. Stdev, standard deviation. Lower panel: MA plot of differential expression of TEs in knockdown and recue embryos, as compared to that in scramble ASO-injected embryos. MERVK elements and MERVL are highlighted.

f) Heatmaps of the expression of 2C-genes in preimplantation embryos, knockdown 2C-embryos, and rescue 2C-embryos.

g) Rain plot displaying the expression change distribution of rescued 2C-genes in double knockdown and recue 2C-embryos.

h) Bar plots showing the expression of representative 2C-genes in knockdown and recue embryos; n=3 biological replicates.

Supplemental figure legends

Supplementary Figure 1

a) Expression profiles of *k*-means clustered gene sets during preimplantation development based on *z*-scored expression of scRNA-seq and bulk RNA-seq. Genes appeared in both scRNA-seq cluster 1 and bulk RNA-seq cluster 4 were designated as 2C-genes.

b) Western blot showing protein products of the candidate genes ectopically expressed in mESCs at 18 hours post transfection.

c) Bar plot showing MERVL transcript level in mESCs at 18 hours post *Dux* or *Obox4* transfection, detected by reverse transcription quantitative real-time PCR (RT-qPCR).

Supplementary Figure 2

a) FACS analysis of 2C::tdTomato cells co-transfected with candidate gene expression plasmids and EGFP.

b) Fluorescence microscopy of 2C::tdTomato ESCs transfected with empty plasmid, plasmid encoding DUX, or plasmid encoding OBOX4. Plasmids encoding EGFP were co-transfected to normalize the transfection efficiency in FACS analysis.

Supplementary Figure 3

a) Schematic diagram of the CUT&RUN workflow using mESCs with induced expression of FLAG-tagged DUX. mESCs bearing a doxycycline-inducible 3×FLAG-OBOX4 expression cassette were induced with doxycycline for 24 h. OBOX4-associated DNA was pulled down in the CUT&RUN assay, using a high-affinity anti-FLAG antibody.

b) Left panel: comparison of DUX binding motif predicted with published ChIP data and CUT&RUN result from this study. Right panel: overlap of DUX binding peaks discovered with the two data sets.

c) Heatmaps showing the OBOX4 binding site distribution near top covered LTR elements.

d) Expression profile of top 5 OBOX4 covered LTR elements during embryogenesis.

Supplementary Figure 4

a) Schematic diagram of producing *Obox4* knockout mice using CRISPR-Cas9 (not drawn to scale). sgRNAs flanking the *Obox4* cluster as well as the internal sequence of individual *Obox4* were introduced into mouse zygotes with SpCas9, to knockout *Obox4*. Primers flanking Cas9 cutting sites (A'-D') were designed to validate removal of target allele. Primers inside of *Obox4* (E'-F') were designed to quantify *Obox4* copy number by qPCR.

b) Schematic diagram of producing *Dux* knockout mice using CRISPR-Cas9 (not drawn to scale). Previously reported sgRNAs flanking the *Dux* cluster were introduced into mouse zygotes with SpCas9, to knockout *Dux*. Primers flanking Cas9 cutting sites (A-D) were used to validate removal of target allele. Primers inside of *Dux* (E-F) were designed to detect translocation of *Dux* cluster.

c) Multiple sequence alignment of DNA sequence among the *Obox4* copies. Full length *Obox4* with internal top codons are marked by asterisks.

d) Schematic diagram of *Obox4* cluster removal strategy and copy number quantification. Primer E' and F' targets all 15 protein-coding as well as 3 non-protein-coding *Obox4* loci, among which 14 protein-coding and 1 non-protein-coding copies were subjected to knockout.

Supplementary Figure 5

a) Agarose gel image of PCR-based genotyping of the *Obox4* knockout allele in founder mESC lines. The red arrows indicate cell lines bearing bi-allelic deletions of the *Obox4* cluster.

b) Agarose gel image of PCR-based genotyping of the *Dux* knockout allele in founder mESC lines. The red arrows indicate cell lines without the genomic *Dux* sequences.

c) Bar plot showing copy number of *Obox4* in the founder mESC lines analyzed in **a-b**, as detected by qPCR using purified genomic DNA.

Supplementary Figure 6

a) Agarose gel image of PCR-based genotyping of the *Obox4* knockout allele in the F_1 mice.

b) Agarose gel image of PCR-based genotyping of the *Dux* knockout allele in the F_1 mice.

c) Agarose gel image of PCR-based genotyping of the *Obox4* cluster 5' cutting site allele in the F_1 mice.

d) Agarose gel image of PCR-based genotyping of the *Dux* cluster 5' cutting site allele in the F_1 mice.

e) Agarose gel image of PCR-based genotyping of the *Dux* internal sequence in the F_1 mice.

f) Bar plot showing copy number of *Obox4* in the F_1 mice analyzed in **a-e**, as detected by qPCR using purified genomic DNA.

Supplementary Figure 7

a) Agarose gel image of PCR-based genotyping of the *Obox4* knockout and *Obox4* cluster 5' cutting site wild type allele in the F_2 mice produced by intercrossing *Obox4*^{Het} F_1 mice.

b) Bar plot showing copy number of *Obox4* in the F_2 mice analyzed in **a**, as detected by qPCR using purified genomic DNA.

Supplementary Figure 8

a) Bar and dot plot showing litter sizes of intercross used to produce *Dux/Obox4* double knockout mice. Each dot represents individual litter size. six and three litters were analyzed for *Dux*^{KO}/*Obox4*^{Het} × *Dux*^{Het}/*Obox4*^{Het} and *Dux*^{KO}/*Obox4*^{Het} × *Dux*^{KO}/*Obox4*^{Het} mating, respectively. Crossing of *Dux*^{KO}/*Obox4*^{Het} × *Dux*^{KO}/*Obox4*^{Het} delivered reduced litter size than those of *Dux*^{KO}/*Obox4*^{Het} × *Dux*^{Het}/*Obox4*^{Het}. * p-value = 0.01104, two-tailed Student's t test. Error bars indicate standard deviations.

b) Agarose gel image of PCR-based genotyping of the *Obox4* knockout, *Obox4* cluster 5' cutting site allele, and *Dux* internal sequence in the F_2 mice produced by intercrossing *Dux*^{KO}/*Obox4*^{Het} and/or *Dux*^{Het}/*Obox4*^{Het} F_1 mice.

c) Bar plot showing copy number of *Obox4* in the F_2 mice analyzed in **a**, as detected by qPCR using purified genomic DNA.

Supplementary Figure 9

a) Schematic diagram of knockout embryo production for development monitoring. *Dux*^{Het}/*Obox4*^{Het} female mice were mated with *Dux*^{KO}/*Obox4*^{Het} male mice. Embryos were collected at 0.5 dpc and cultured *in vitro* until 4.5 dpc, followed by developmental assessment and genotyping.

b) Agarose gel image of multiplex PCR-based genotyping of *Obox4* cluster 5' cutting site allele, *Dux* internal sequence, and *Tardbp* internal sequence in the embryos produced by intercrossing *Dux*^{KO}/*Obox4*^{Het} and *Dux*^{Het}/*Obox4*^{Het} F_1 mice. Note that multiplexing three sets of PCR primers produced artifact band in *Dux*^{KO}/*Obox4*^{KO} embryos.

c) Representative pictures of *Dux*^{KO}/*Obox4*^{KO} embryos.

455 d) Schematic diagram of knockout embryo production for RNA-seq. Embryos were collected at 0.5 dpc from
456 *Dux*^{KO}/*Obox4*^{Het} mating pairs and cultured *in vitro* until 2-cell stage at 1.5 dpc, blastomeres of each embryo were
457 separated and subject to genotyping and RNA-seq respectively.
458 e) Agarose gel image of genotyping of *Obox4* cluster 5' cutting site allele in the embryos produced by intercrossing
459 *Dux*^{KO}/*Obox4*^{He} mice.
460
461 **Supplementary Figure 10**
462 a) Transcript levels of *Dux* and *Obox4* in ASO-injected embryos, as measured using RNA-seq. CPM, counts per
463 million.
464 b) Representative images of immunofluorescence co-staining of OBOX4 and DUX in 2C embryos subjected to
465 ASO-mediated knockdown.
466 c) Dot plots showing the per-nucleus intensity of OBOX4 and DUX normalized to dapi.
467 d) Heatmaps of the expression of morula-genes in preimplantation embryos and knockdown morulae. Genes
468 appeared in both scRNA-seq cluster 6 and bulk RNA-seq cluster 3 in Supplementary Fig. 1a were designated as
469 morula-genes.
470 e) Transcriptome-based PCA of knockdown morulae and preimplantation embryos.
471 f) Volcano plot of DEGs in double knockdown morulae comparing with scramble knockdown. Selected apoptosis
472 associated genes are highlighted.
473 g) The enrichment of gene ontology (GO) terms of up-regulated genes in double knockdown morulae.
474
475 **Supplementary Figure 11**
476 a) Schematic of the production of monoclonal antibodies. Mice were immunized with the GST-OBOX4 fusion
477 protein. After fusing B-cells with myelomas, the antibodies produced by hybridomas were examined against MBP-
478 OBOX4 fusion protein, followed by MBP-OBOX2 fusion protein, for identification of OBOX4-specific antibodies.
479 b) Analysis of protein sequence similarity among the OBOX family members. The Smith–Waterman local alignment
480 method was used to align the amino acid sequences, and the divergence among different sequences was represented
481 in the form of a block substitution matrix.
482 c) ELISA signal of anti-OBOX4 monoclonal antibodies against the MBP-OBOX4 and MBP-OBOX2 fusion
483 proteins. Anti-OBOX4 monoclonal antibodies were not reactive to MBP-OBOX2.
484 d) Multiple sequence alignment of protein sequence among the OBOX family members. The homeodomains are
485 highlighted by magenta box. The peptide sequences used for antibody production are highlighted by black box.
486

487 # Methods

488 **Mice**

489 Male/female BDF1 and female BALB/c mice were purchased from Japan SLC Inc. Mice were fed regular chow
490 and housed in a controlled room under a 14 h/10 h light/dark cycle, at 22°C. All animal experiments were approved
491 by the Animal Care and Use Committee of Keio University and the Animal Experimentation Committee at the RIKEN

492 Tsukuba Institute and conducted in compliance with the Keio University Code of Research Ethics and the RIKEN's
493 guiding principles.
494
495 **Cell culture**
496 All mouse mESC lines were cultured in Dulbecco's Modified Eagle Medium (DMEM) (catalog no. 08488-55,
497 Nacalai Tesque) supplemented with 10% fetal bovine serum (lot no. S10581S1820, Biowest), 1× GlutaMAX™ (catalog
498 no. 35050061, Gibco), 1× penicillin-streptomycin (catalog no. 15140163, Gibco), 1× non-essential amino acids (catalog
499 no. 11140050, Gibco), 1× sodium pyruvate (catalog no. S8636, Merck), 50 μM 2-mercaptoethanol (catalog no.
500 21985023, Gibco), 1 μM CHIR99021 (catalog no. 034-23103, Wako), 3 μM PD0325901 (catalog no. 168-25293, Wako),
501 and mouse leukemia inhibitory factor produced in-house. The culture medium was supplemented with iMatrix-511 silk
502 (recombinant human laminin-511 E8 fragment) (catalog no. 892021, Matrixome) at a concentration of 125 ng.cm^{-2}
503 culture vessel area, before seeding mESCs into it. The cells were cultured in a humidified atmosphere containing 5%
504 CO_2 at 37°C, with the media changed every 48 h.
505 TBLCs were generated by culturing mESCs in an ordinary medium supplemented with 2.5 nM PLaB (catalog no.
506 16538, Cayman Chemicals). Cells were sub-cultured every 2–4 d, at a seeding density of 1×10^5 cm^{-2} culture vessel area.
507 After five rounds of sub-culture, the cells were deemed TBLCs.
508 SP2/O-Ag14 myeloma and primary clones of hybridomas were cultured in GIT medium (catalog no. 63725715,
509 Wako) supplemented with recombinant human interleukin-6 (IL-6) (catalog no. 20006, PeproTech). Cells were cultured
510 in a humidified atmosphere containing 5% CO_2 at 37°C and sub-cultured every day, at a seeding density of 3×10^5 mL^{-}
511 ^{1}. For monoclonal antibody production, hybridomas were cultured in hybridoma serum-free medium supplemented
512 with IL-6. The cells were cultured in a humidified atmosphere containing 5% CO_2 at 37°C, until they were over-
513 confluent.
514
515 **Cell transfection**
516 Plasmid transfections were performed using jetOPTIMUS® DNA Transfection Reagent (catalog no. 101000025,
517 Polyplus), according to the manufacturer's instructions. Briefly, mESCs were seeded at a cell density of 8×10^4 cm^{-2}
518 culture vessel area. After 20 min, the jetOPTIMUS® reagent and plasmids were diluted in jetOPTIMUS® buffer,
519 incubated for 10 min at room temperature, and then applied to the cell culture. After 48 h, the cells were collected for
520 downstream experiments.
521
522 **cDNA synthesis and cloning**
523 Total RNA was extracted from TBLCs using ISOGEN (catalog no. 311-02501, Nippon Gene), according to the
524 manufacturer's instructions. Briefly, 500 μL ISOGEN was added to 1.5×10^6 freshly harvested TBLCs. After 5 min of
525 incubation at room temperature, 100 μL of chloroform (catalog no. 03802606, Wako) was added to the cells and mixed
526 by means of vigorous shaking. After 2 min of incubation at room temperature, the samples were centrifuged at 12,000
527 × *g* for 15 min at 4°C. The upper aqueous phase was then transferred to a new tube and mixed with 240 μL isopropanol
528 (catalog no. 15-2320, Merck), to precipitate the RNA. After 5 min of incubation at room temperature, the samples were
529 centrifuged at 12,000 × *g* for 15 min at 4°C. The supernatant was then discarded, following which the RNA pellets
530 were washed with 70% ethanol (catalog no. 057-00456, Wako). The RNA pellets were then air-dried and dissolved in

531 RNase-free water. The RNA solution was subjected to DNase treatment using TURBO DNA-*free*™ kit (catalog no.
532 AM1907, Thermo Fisher), according to the manufacturer's instructions, to remove genomic DNA carryover. RNA (1
533 μg) was reverse transcribed to cDNA using the Transcriptor First Strand cDNA Synthesis Kit (catalog no. 04379012001,
534 Roche), according to the manufacturer's instructions. PrimeSTAR® Max DNA Polymerase (catalog no. R045A,
535 TaKaRa) and ProFlex™ PCR System (catalog no. 4484073, Thermo Fisher) were used to amplify the sequence of
536 interest from the cDNA. NEBuilder® HiFi DNA Assembly Kit (catalog no. E2621L, NEB) was used to clone the
537 sequence of interest into plasmid backbone.
538
539 **Immunofluorescence**
540 For embryos, middle-2C-embryos were collected at 1.5 dpc. The zona pellucida was removed by treating the
541 embryos with acidic Tyrode's solution (catalog no. MR-0040-D, Merck). The embryos were fixed in 4%
542 paraformaldehyde (catalog no. 09154-14, Nacalai Tesque) in PBS for 10 min. Following three washes in PBS, fixed
543 embryos were permeabilized with 0.1% Triton™ X-100 (catalog no. 1610407, Bio-Rad) in PBS, for 20 min at room
544 temperature. Following three washes in PBS, permeabilized embryos were blocked in 2% bovine serum albumin (BSA;
545 catalog no. 011-27055, Wako) in PBS, for 20 min at room temperature. The blocked embryos were incubated with
546 primary antibodies diluted in 2% BSA in PBS, at 4°C overnight. Following three washes in PBS, the embryos were
547 incubated with 2% BSA in PBS containing 1:200 diluted 4′,6-diamidino-2-phenylindole (DAPI) (catalog no. 19178-91,
548 Nacalai Tesque) and 1:500 diluted Alexa Fluor™-conjugated anti-mouse IgG1 secondary antibody (catalog no. A-
549 21127, Thermo Fisher) or Alexa Fluor™-conjugated anti-mouse IgG2a secondary antibody (catalog no. A-21131,
550 Thermo Fisher) and, for 1 h at room temperature. Following three washes in PBS, the embryos were transferred into
551 liquid paraffin-covered PBS drops on a glass-bottom dish (catalog no. D11130H, Matsunami).
552 For culturing, cells seeded on glass bottom chamber slides (catalog no. SCS-N02, Matsunami) were fixed with 4%
553 paraformaldehyde in PBS, for 10 min. After three washes in PBS, the fixed cells were permeabilized with 0.1% Triton™
554 X-100 in PBS, for 15 min at room temperature. Following three washes in PBS, permeabilized cells were incubated
555 with primary antibodies diluted with 2% skim milk in PBS, for 30 min at room temperature. Following three washes in
556 PBS, the cells were incubated with 2% BSA in PBS containing 1:500 diluted Alexa Fluor™-conjugated secondary
557 antibody and 1:200 diluted DAPI, for 1 h at room temperature. Following three washes in PBS, the chamber was
558 removed and the slides were mounted with ProLong™ Glass Antifade Mountant (catalog no. P36982, Thermo Fisher).
559 Fluorescence images were taken using a confocal laser scanning microscope (catalog no. FV3000, Olympus).
560
561 **Western blot**
562 Freshly harvested cells were re-suspended in phosphate-buffered saline (PBS) (catalog no. 14249-95, Nacalai
563 Tesque) and lysed by means of sonication. Whole cell lysates were mixed with sample buffer containing reducing reagent
564 (catalog no. 09499-14, Nacalai Tesque) and boiled at 95°C for 5 min. Protein samples were loaded on a 10% tris-
565 glycine gel, run in AllView PAGE Buffer® (catalog no. DS520, BioDynamics Laboratory), and then transferred to
566 nitrocellulose membranes (catalog no. 10600003, Cytiva) using a Power Blotter System (catalog no. PB0012, Thermo
567 Fisher). The membranes were blocked with PBST containing 2% skim milk (catalog no. 4902720131292, Morinaga),
568 at room temperature for 15 min. Membranes were incubated with primary antibodies in PBST containing 2% skim
569 milk, at room temperature for 30 min. After three washes with PBST, the membrane was incubated with secondary

570 antibodies in PBST containing 2% skim milk, at room temperature for 15 min, with shaking. After three washes with
571 PBST, the membrane was incubated with ECL reagents (catalog no. RPN2232, Cytiva) and exposed to an X-ray film
572 (catalog no. 28906839, Cytiva) or detected using a digital chemiluminescence imager (catalog no. 17001402JA, Bio-
573 Rad).
574
575 **qPCR**
576 qPCR was performed using TB Green Fast qPCR Mix (catalog no. RR430A, TaKaRa) according to the
577 manufacturer's instructions. The qPCR reactions were carried out and the signals were detected using a real time PCR
578 system (catalog no. TP950, TaKaRa). For RT-qPCR, first strand cDNA of mESCs total RNA was produced as
579 described in methods **cDNA synthesis and cloning** section. Primers targeting MERVL Gag consensus sequence
580 were used to detect MERVL transcript. Primers targeting beta actin mRNA were used as internal control in all qPCR
581 assays performed in this study.
582
583 **smFISH**
584 smFISH probes targeting MERVL were designed and synthesized by LGC Biosearch Technologies as previously
585 described [59]. smFISH followed by immunofluorescence staining was performed according to the manufacturer's
586 instructions. Briefly, Quasar 570 labeled probes were hybridized against MERVL RNA at 37°C for 16 h. Followed by
587 immunofluorescence staining described in methods **Immunofluorescence** section, without blocking step to prevent
588 RNase contamination. The slides were mounted with ProLong™ Glass Antifade Mountant (catalog no. P36982,
589 Thermo Fisher). Fluorescence images were taken using a confocal laser scanning microscope (catalog no. FV3000,
590 Olympus).
591
592 **Flow cytometry**
593 The cells were digested with 0.25% trypsin-EDTA (catalog no. 25200072, Gibco), at 37°C for 5 min, and then re-
594 suspended in FluoroBrite™ DMEM (catalog no. A1896701, Gibco). The cell suspension was filtered through a 35 μM
595 cell strainer (catalog no. 352235, Falcon). The samples were analyzed using a cell sorter (catalog no. SH800Z, Sony).
596 Data analysis was performed using the Sony SH800Z cell sorter software.
597
598 **Generation of transgenic mESC lines**
599 The 2C::tdTomato reporter cell line was generated by transfection of EB3 mESCs (catalog no. AES0139, RIKEN
600 BRC Cell Bank) with a linearized 2C::tdTomato reporter plasmid (catalog no. 40281, Addgene). After 48 h, the cells
601 were subjected to 500 $\mu g.mL^{-1}$ hygromycin (catalog no. 08906151, Wako) for 7 d. The selected cells were then seeded
602 at a density of 2×10^2 cm^{-2} in culture medium containing 250 $\mu g.mL^{-1}$ hygromycin. Single-cell clones were picked and
603 expanded after 7 d.
604 A tetracycycline-controlled transcription activation system and a piggyBac transposon system were used as
605 previously described [60], to generate an *Obox4*-inducible cell line. Briefly, pPB-TRE-3×FLAG-Obox4, pPB-CAG-
606 rtTA3G-IRES-Hygro, and pCMV-HyPBase-PGK-Puro plasmids were co-transfected into EB3 mESCs. After 48 h, the
607 cells were subjected to selection with 500 $\mu g.mL^{-1}$ hygromycin and 500 $\mu g.mL^{-1}$ G418 (catalog no. 07805961, Wako),

608 for 7 d. The selected cells were then seeded at a density of 2×10^2 cm^{-2} in a culture medium containing 250 μg.mL^{-1}
609 hygromycin and 250 μg.mL^{-1} G418. Single-cell clones were picked and expanded after 7 d.
610
611 **Generation of monoclonal antibodies**
612 The anti-OBOX4, anti-DUX, and anti-GAG monoclonal antibodies were produced as previously described [61]
613 (Supplementary Fig. 11a). Briefly, BALB/c mice were immunized by means of intraperitoneal injection of glutathione
614 S-transferase-fused protein-of-interest (PoI). The mice were routinely immunized until their sera tested positive for the
615 PoI-fused maltose binding protein (MPB), after which two boosting immunizations were performed. Following boosting,
616 splenocytes from immunized mice were fused with SP2/O myeloma and cultured in hypoxanthine-aminopterin-
617 thymidine medium for 10 d, to select for hybridomas. Hybridomas were subsequently screened using enzyme-linked
618 immunosorbent assay against PoI-fused MBP. The positive polyclonal hybridomas were monoclonalized and expanded.
619 For anti-OBOX4 hybridomas, additional screening using OBOX2-fused MBP was conducted. The sequence of
620 OBOX4 was significantly divergent from those of other OBOX members, and the monoclonal antibodies were negative
621 for cross-reactivity with OBOX2 (Supplementary Fig. 11b-c). The N-terminal 100 amino acids of OBOX4 and
622 OBOX2 were used for immunization and cross-reactivity examination respectively (Supplementary Fig. 11d). The
623 culture supernatants of monoclonal hybridomas were sterilized by passing them through a 0.22 μM pore size filter
624 (catalog no. 430769, Corning) and used directly as an antibody solution in other assays.
625
626 **Generation of knockout mouse lines**
627 Single guide RNAs (sgRNAs) designed on flanking and inside of the *Obox4* cluster were synthesized using a
628 Precision gRNA Synthesis Kit (catalog no. A29377, Thermo Fisher) according to the manufacturer's instructions. 150
629 ng.mL^{-1} sgRNA and 125 ng/μL Alt-R S.p. Cas9 Nuclease (catalog no. 1081058, Integrated DNA Technologies) diluted
630 with Hepes-buffered KSOM were electroporated into BDF1 × B6 *in vitro* fertilized embryos with an electroporator
631 (catalog no. NEPA21, NEPA GENE). Treated embryos were cultured in KSOM for 18 h and embryos that reached
632 the two-cell stage were transferred into the oviducts of pseudopregnant ICR female mice on day 0.5. Pups were retrieved
633 on day 19.5 and genotyped with specific PCR primers.
634
635 **Generation of knockout mESC lines**
636 Plasmids encoding Cas9 and single guide RNA (sgRNA) flanking and inside of the *Obox4* cluster were constructed
637 to perform knockout experiment. The *Obox4* knockout cell line was generated by means of co-transfection of EB3
638 mESCs with the pX330-Puro-Obox4KO-3, pX330-Puro-Obox4KO-4, pX330-Puro-Obox4KO-6, and pX330-Puro-
639 Obox4KO-7 plasmids. After 18 h, the cells were subjected to selection with 1 μg.mL^{-1} puromycin (catalog no. 16023151,
640 Wako) for 54 h. The selected cells were then seeded at a very low density in culture medium without antibiotics. Single-
641 cell clones were picked and expanded after 7 d, and then subjected to genotyping.
642 Following a previously published protocol [18], plasmids encoding Cas9 and sgRNAs flanking the *Dux* cluster were
643 constructed to perform knockout experiment. The *Dux* knockout cell line and the *Obox4/Dux* double knockout cell line
644 were generated by means of co-transfection of EB3 mESCs and *Obox4* knockout cell lines with pX330-DuxKO-A and
645 pX330-DuxKO-B plasmids. After 48 h, the cells were seeded at a very low density. Single-cell clones were picked and
646 expanded after 7 d and then subjected to genotyping.

647 While mono-allelic *Obox4* deletion was detected in 49.1% (335/682) of the CRISPR-Cas9 edited clones, bi-allelic
648 deletion was only detected in 0.44% (3/682) of the population, suggesting that removal of *Obox4* allele was associated
649 with severe genetic toxicity. In contrast, 36.7% (47/128) mono-allelic and 4.7% (6/128) bi-allelic deletions were
650 detected in *Dux* knockout clones.
651
652 **Genotyping and copy number examination**
653 For mouse and culture cell, mouse right hindlimb toe or tail tip, or 1×10^6 culture cells were incubated in 400 μL
654 ProK solution containing 20 mM Tris-HCl pH = 7.9, 1 mM EDTA, 1% w/v sodium dodecyl sulfate (SDS), 150 mM
655 NaCl, 20 mM trisodium citrate, and 80 μg recombinant proteinase K (catalog no. 161-28701, Wako) at 55°C for 2 h
656 with vigorous shaking. The solution was extracted with 2 volumes of phenol/chloroform/isoamyl alcohol (25:24:1)
657 (catalog no. 311-90151, Nippon Gene) twice. DNA in the aqueous phase was precipitated by adding 0.1 volume of 3
658 M sodium acetate and 2 volumes of 99.5% ethanol (catalog no. 057-00456, Wako), snap freeze in liquid nitrogen, and
659 centrifuged at 15,000 × *g* for 12 min at 4°C. After discarding supernatant, the DNA pellets were washed by 200 μL 70%
660 ethanol, air dried at room temperature, and dissolved in 220 μL TE solution (Tris-HCl pH = 7.9, 1 mM EDTA)
661 supplemented with 1 μg RNase A (catalog no. 131-01461, Nippon Gene). The solution was incubated at 37°C for 1 h,
662 then phenol/chloroform/isoamyl alcohol extracted and ethanol precipitated again as described above, to obtain highly
663 purified genomic DNA. The DNA was dissolved in 200 μL TE solution.
664 For single blastomeres and abnormal embryos, whole genome amplifications were performed on individual
665 embryos by using REPLI-g Advanced DNA Single Cell Kit (catalog no. 150363, Qiagen) according to the
666 manufacturer's instructions. For blastocysts, crude genomic DNA from single blastocysts was prepared according to the
667 method described by Sakurai *et al.*[62] with some modifications. Briefly, single blastocysts in 0.5 μL KSOM medium were
668 transferred to the bottom of 0.1 mL PCR tubes, followed by addition of 10 μL blastocyst lysis buffer containing of 120
669 μg/mL recombinant proteinase K, 100mM Tris-HCl pH = 7.9, 100mM KCl, 0.45% NP-40, and 10 μg/mL yeast
670 tRNA (catalog no. AM7119, Thermo Fisher). After brief vortex and pulse spin, the tubes were incubated at 55°C for
671 10 min followed by 95°C for 10 min.
672 For PCR based genotyping, 10 ng purified genomic DNA, 10ng whole genome amplified DNA, or 2μL of
673 blastocyst lysate were used as template and amplified with target specific primers by KOD One® PCR Master Mix
674 (catalog no. KMM-101, TOYOBO) according to the manufacturer's instructions. Primers targeting mouse *Tardbp* were
675 used as internal control when whole genome amplification product or blastocyst lysate were used as multiplex PCR
676 template. For copy number examination, 5 ng genomic DNA template was amplified as described in methods **qPCR**
677 section.
678
679 ***In vitro* transcription**
680 The *Obox4* coding sequence was codon-optimized using GeneArt Instant Designer (Thermo Fisher), to remove the
681 ASO target motif and improve translation efficiency. Codon-optimized DNA was synthesized using Prime Gene
682 Synthesis Services (Thermo Fisher). Codon-optimized *Obox4* mRNA was transcribed *in vitro* using the mMESSAGE
683 mMACHINE™ T7 Transcription Kit (catalog no. AM1344, Thermo Fisher) and then polyadenylated using a poly(A)
684 tailing kit (catalog no. AM1350, Thermo Fisher), according to the manufacturer's instructions. The polyadenylated

mRNA was purified using the RNeasy Mini Kit (catalog no. 74004, Qiagen), according to the manufacturer's instructions, and dissolved in RNase-free water, at a concentration of 100 ng.μL^{-1}.

Pronuclear injection of mouse embryos

Eight-week-old BDF1 female mice were injected with 150 μL of CARD HyperOva (catalog no. KYD-010-EX, Kyudo Co., Ltd.). After 48 hours, the female mice were injected with 5 IU human chorionic gonadotropin (hCG) (catalog no. GONATROPIN, ASKA Animal Health Co. Ltd.) and mated with BDF1 male mice. After 22 h, the PN3 zygotes were collected. Cumulus cells were removed by briefly culturing the zygotes in potassium simplex optimization medium (KSOM) (catalog no. MR-101-D, Merck) supplemented with 0.3 μg.μL^{-1} hyaluronidase (catalog no. H4272, Merck). Embryos were cultured in KSOM medium drops covered with liquid paraffin (catalog no. 26137-85, Nacalai Tesque), in a humidified atmosphere with 5% CO_2, at 37°C. After 4 h, PBS containing either 40 μM scramble ASO, 20 μM anti-*Dux* ASO, 20 μM anti-*Obox4* ASO, 40 μM equimolar anti-*Dux*/anti-*Obox4* ASO mixture, or 40 μM equimolar anti-*Dux*/anti-*Obox4* ASO mixture with 100 ng.μL^{-1} codon-optimized *Obox4* mRNA was microinjected into the male pronuclei of zygotes using a microinjector (catalog no. 5252000013, Eppendorf). For developmental monitoring, embryos were cultured for 4 d after microinjection and assessed for developmental stage at 18 h, 42 h, 66 h, and 90 h after microinjection, which corresponded to 1.5 dpc, 2.5 dpc, 3.5 dpc, and 4.5 dpc, respectively.

Somatic cell nuclear transfer (SCNT)

SCNT was performed as described previously [63] using wild-type and knockout mESC lines as nuclear donor cells. They were cultured at a high density until they reached confluency for about four to six days before SCNT. BDF1 female mice were superovulated by the injection of 7.5 IU of equine chorionic gonadotropin (eCG, ZENOAQ) and 7.5 IU of hCG (ASKA Pharmaceutical Co., Ltd.) at a 48 h interval. At 15 h after hCG injection, cumulus–oocyte complexes were collected from the oviducts. After removal of cumulus cells by 0.1% bovine testicular hyaluronidase (catlog no. 385931, Calbiochem), oocytes were enucleated in Hepes-buffered KSOM containing 7.5 μg/mL cytochalasin B. After culture in KSOM for at least 1 h, the enucleated oocytes were injected with donor mESCs using a Piezo-driven micromanipulator (catalog no. PMM-150FU, Primetech). After culture in KSOM for about 1 h, injected oocytes were cultured in Ca^{2+}-free KSOM containing 2.5 mM $SrCl_2$, 5 μM latrunculin A (LatA) (catalog no. L5163, Merck) with 50 nM trichostatin A (TSA) (catalog no. T8552, Merck) for 1 h. Then, they were cultured in KSOM containing 5 μM LatA and 50 nM TSA for 7 h. After washing, the SCNT embryos were cultured in KSOM under 5% CO_2 in air at 37°C for 96 h. The embryos that reached 2-cells at 24 h after activation were considered successfully cloned with cell cycle-matched mESCs (G0/G1 phase).

scRNA-seq analysis

Raw scRNA-seq data was obtained from the dataset of Deng et al. (GSE45719). Quality control and adapter trimming was done using fastp [64] v0.23.2. Quality-controlled reads were aligned to the GRCm38.p6 reference genome using STAR [65] v2.7.9a, with default arguments. Reads were counted against GRCm38.p6 comprehensive gene annotation [66] and mm10 repeats from the University of California, Santa Cruz (UCSC) RepeatMasker using Subread [67] v2.0.1 featureCounts function, and multi-mapping reads were discarded for non-TE features and counted fractionally for TEs. Seurat [68] v4.1.0 was used to process the read counts of scRNA-seq. Cells with greater than 7.5% mitochondrial

724 reads or less than 14,000 annotated features were discarded. Expression levels were log-normalized. The expression
725 profiles of homeobox genes listed in HomeoDB2 [69] were clustered into 11 *k*-means after *z*-score transformation.
726
727 **Ribo-seq analysis**
728 Raw Ribo-seq data was obtained from the dataset of Xiong et al. (GSE165782). Reads were quality-controlled,
729 aligned, and counted, as described above. Reads aligned to all protein coding *Obox4* loci were added up to represent
730 translation level of OBOX4.
731
732 **Bulk RNA-seq**
733 For embryos, 30 middle-2C-embryos were collected 20 h after microinjection in each independent biological
734 replicate. The zona pellucida was removed by treating embryos with acidic Tyrode's solution. Libraries were
735 constructed using the SMART-Seq® Stranded Kit (catalog no. 634442, TaKaRa) and indexed using the SMARTer®
736 RNA Unique Dual Index Kit (catalog no. 634451, TaKaRa), according to the manufacturer's instructions.
737 For cell culture, total RNA was prepared using the RNeasy Kit, according to the manufacturer's instructions. The
738 RNA solution was subjected to DNase treatment to remove genomic DNA carryover. Using 1 μg total RNA per sample,
739 libraries were constructed with the NEBNext® Ultra™ II Directional RNA Library Prep Kit for Illumina (catalog no.
740 E7760L, NEB) and indexed with NEBNext® Multiplex Oligos for Illumina (catalog no. E6440S, NEB), according to
741 the manufacturer's instructions.
742 The libraries were quantified with a 2100 Bioanalyzer (catalog no. G2939BA, Agilent) using a High Sensitivity
743 DNA Kit (catalog no. 5067-4626, Agilent). Quantified libraries were pooled and sequenced using an Illumina NovaSeq
744 6000 System in 150 bp paired-end mode (Illumina). Base calling and de-multiplexing were performed using the
745 bcl2fastq2 (Illumina) v2.20. De-multiplexed reads were quality-controlled, aligned, and counted, as described above.
746 DESeq2 [70] v1.32.0 was used to perform differential expression analysis. Raw RNA-seq reads for TBLCs were
747 downloaded from the dataset of Shen et al. (GSE168728). Raw RNA-seq reads of *Dux* knockout embryos were
748 downloaded from the datasets of Chen & Zhang and De Iaco et al. (GSE121746 and GSE141321 respectively). Raw
749 RNA-seq reads of preimplantation embryos were downloaded from the datasets of Wu et al. (GSE66390). Raw RNA-
750 seq reads of 2C-like mESCs were downloaded from the datasets of Zhu et al. (GSE159623). The published data were
751 analyzed using the same method.
752
753 **CUT&RUN-seq**
754 Cultured cells (1×10^5) freshly prepared by trypsin-EDTA digestion were used to perform CUT&RUN with the
755 CUT&RUN Assay Kit (catalog no. 86652, Cell Signaling Technology), according to the manufacturer's instructions.
756 Enriched DNA was subjected to library construction using the NEBNext® Ultra™ II DNA Library Prep Kit for
757 Illumina (catalog no. E7645L, NEB), with the adapter ligation step performed at 50°C instead of 65°C, to prevent the
758 denaturation of small DNA inserts. The libraries were indexed using NEBNext® Multiplex Oligos for Illumina,
759 according to the manufacturer's instructions.
760 The libraries were quantified, pooled, sequenced, de-multiplexed, and quality controlled, as described above.
761 Processed reads were aligned to the GRCm38.p6 reference genome using Bowtie2 [71] v2.4.1, with default settings. Peaks
762 were called in each biological replicate using the MACS3 [72] v3.0.0a6 callpeak function (-f BAMPE). Alignment tracks

were first generated using deepTools [73] v3.5.1 bamCoverage function (--binSize 10 --normalizeUsing CPM --smoothLength 30), and then normalized by subtracting the signal from non-immune IgG and wildtype mESCs using the deepTools bamCompare function (--scaleFactorsMethod None --operation subtract --binSize 10 --smoothLength 30). ChIPseeker [74] v1.28.3 was used to annotate the peaks. The MEME suite [75] v5.4.1 was used to identify the binding motifs. Heatmaps were generated using deepTools computeMatrix and plotHeatmap functions. Visualization of genomic tracks was performed using trackplot [76] v1.3.10. Raw ChIP-seq reads of DUXs in mESCs were downloaded from Hendrickson et al. (GSE85632). The published data were analyzed using the same method.

Quantification and statistical analysis

Descriptive and comparative statistics were employed in the manuscript as described in the figure legends with the number of replicates indicated. Significance is defined as a *p-value* less than 0.05 indicated with asterisk (* *p-value* < 0.05, ** *p-value* < 0.01, *** *p-value* < 0.001). Error bar represents the standard deviation (SD) of the mean of the replicates.

Data and code availability

The RNA-seq and CUT&RUN-seq data generated in this study have been deposited at NCBI Gene Expression Omnibus (GEO) database under the accession code GSE196671.

Acknowledgements

We thank all the members of the Siomi Laboratory for their discussions and comments on this work. We thank Takehiko Yokomizo (Department of Biochemistry, Juntendo University) for providing the anti-DYKDDDDK monoclonal antibody (clone 2H8). We also thank Daisuke Motooka (Research Institute for Microbial Diseases, Osaka University) for generating the sequencing data. We are grateful to Azusa Inoue (Center for Integrative Medical Sciences, RIKEN) and Katsuhiko Hayashi (Department of Genome Biology, Osaka University) for their comments on this manuscript. This work was supported by the MEXT Grant-in-Aid for Scientific Research in Innovative Areas (19H05753 to H.S. and 19H05758 to A.O.), AMED project to elucidate and control mechanisms of aging and longevity (1005442 to H.S.), JSPS Grant-in-Aid for Scientific Research KAKENHI (20K21507 to K.M. and 22H02534 to K.I.), Mochida Memorial Foundation Research Grant to K.M., Sumitomo Foundation Research Grant to K.M., Keio University Doctorate Student Grant-in-Aid Program to Y.G., and the JST Doctoral Program Student Support Fellowship to Y.G.

Author contributions

H.S. and Y.G. conceived and designed the project; Y.G., T.K., K.M., T.D.L., A.S., H.I., N.O., S.M., M.S., and A. O. performed the experiments; Y.G. and T.K. analyzed the data; H.I. developed the ASO-mediated knockdown experiments; H.S. and K.M. supervised and coordinated the experiments; Y.G. and H.S. wrote the paper with input from all authors. All authors reviewed and approved the final version of the manuscript.

Declaration of interests

The authors declare no competing interests.

References

1. Lee, M.T., Bonneau, A.R. & Giraldez, A.J. Zygotic genome activation during the maternal-to-zygotic transition. *Annual review of cell and developmental biology* **30**, 581-613 (2014).
2. Tarkowski, A.K. Experiments on the development of isolated blastomeres of mouse eggs. *Nature* **184**, 1286-1287 (1959).
3. Tarkowski, A.K. Experimental studies on regulation in the development of isolated blastomeres of mouse eggs; Badania eksperymentalne nad rozwojem izolowanych blastomerów jaj myszy. *Acta Theriologica* **3**, 191-267 (1959).
4. Suwińska, A., Czołowska, R., Ożdżeński, W. & Tarkowski, A.K. Blastomeres of the mouse embryo lose totipotency after the fifth cleavage division: expression of Cdx2 and Oct4 and developmental potential of inner and outer blastomeres of 16-and 32-cell embryos. *Developmental biology* **322**, 133-144 (2008).
5. Svoboda, P. *et al.* RNAi and expression of retrotransposons MuERV-L and IAP in preimplantation mouse embryos. *Developmental biology* **269**, 276-285 (2004).
6. McGinnis, W., Levine, M.S., Hafen, E., Kuroiwa, A. & Gehring, W.J. A conserved DNA sequence in homoeotic genes of the Drosophila Antennapedia and bithorax complexes. *Nature* **308**, 428-433 (1984).
7. Carrasco, A.E., McGinnis, W., Gehring, W.J. & De Robertis, E.M. Cloning of an X. laevis gene expressed during early embryogenesis coding for a peptide region homologous to Drosophila homeotic genes. *Cell* **37**, 409-414 (1984).
8. McGinnis, W., Hart, C.P., Gehring, W.J. & Ruddle, F.H. Molecular cloning and chromosome mapping of a mouse DNA sequence homologous to homeotic genes of drosophila. *Cell* **38**, 675-680 (1984).
9. Scott, M.P. & Weiner, A.J. Structural relationships among genes that control development: sequence homology between the Antennapedia, Ultrabithorax, and fushi tarazu loci of Drosophila. *Proceedings of the National Academy of Sciences* **81**, 4115-4119 (1984).
10. Gehring, W.J. & Hiromi, Y. Homeotic genes and the homeobox. *Annual review of genetics* **20**, 147-173 (1986).
11. Gehring, W.J. Homeo boxes in the study of development. *Science* **236**, 1245-1252 (1987).
12. Lewin, T.D., Royall, A.H. & Holland, P.W. Dynamic Molecular Evolution of Mammalian Homeobox Genes: Duplication, Loss, Divergence and Gene Conversion Sculpt PRD Class Repertoires. *Journal of Molecular Evolution*, 1-19 (2021).
13. Töhönen, V. *et al.* Novel PRD-like homeodomain transcription factors and retrotransposon elements in early human development. *Nature communications* **6**, 8207 (2015).
14. Madissoon, E. *et al.* Characterization and target genes of nine human PRD-like homeobox domain genes expressed exclusively in early embryos. *Scientific reports* **6**, 1-14 (2016).
15. De Iaco, A. *et al.* DUX-family transcription factors regulate zygotic genome activation in placental mammals. *Nature genetics* **49**, 941-945 (2017).
16. Hendrickson, P.G. *et al.* Conserved roles of mouse DUX and human DUX4 in activating cleavage-stage genes and MERVL/HERVL retrotransposons. *Nature genetics* **49**, 925-934 (2017).
17. Whiddon, J.L., Langford, A.T., Wong, C.-J., Zhong, J.W. & Tapscott, S.J. Conservation and innovation in the DUX4-family gene network. *Nature genetics* **49**, 935-940 (2017).
18. Chen, Z. & Zhang, Y. Loss of DUX causes minor defects in zygotic genome activation and is compatible with mouse development. *Nature genetics* **51**, 947-951 (2019).

841 19. Guo, M. *et al.* Precise temporal regulation of Dux is important for embryo development. *Cell research* **29**, 956-959
842 (2019).
843 20. De Iaco, A., Verp, S., Offner, S., Grun, D. & Trono, D. DUX is a non-essential synchronizer of zygotic genome
844 activation. *Development* **147**, dev177725 (2020).
845 21. Bosnakovski, D., Gearhart, M.D., Ho Choi, S. & Kyba, M. Dux facilitates post-implantation development, but is
846 not essential for zygotic genome activation. *Biology of reproduction* **104**, 83-93 (2021).
847 22. Shen, H. *et al.* Mouse totipotent stem cells captured and maintained through spliceosomal repression. *Cell* **184**, 2843-
848 2859. e20 (2021).
849 23. Wagner, A. Genetic redundancy caused by gene duplications and its evolution in networks of transcriptional
850 regulators. *Biological cybernetics* **74**, 557-567 (1996).
851 24. Deng, Q., Ramsköld, D., Reinius, B. & Sandberg, R. Single-cell RNA-seq reveals dynamic, random monoallelic
852 gene expression in mammalian cells. *Science* **343**, 193-196 (2014).
853 25. Howe, K.L. *et al.* Ensembl 2021. *Nucleic Acids Research* **49**, D884-D891 (2020).
854 26. Xiong, Z. *et al.* Ultrasensitive Ribo-seq reveals translational landscapes during mammalian oocyte-to-embryo
855 transition and pre-implantation development. *Nature Cell Biology* **24**, 968-980 (2022).
856 27. Macfarlan, T.S. *et al.* Endogenous retroviruses and neighboring genes are coordinately repressed by LSD1/KDM1A.
857 *Genes & development* **25**, 594-607 (2011).
858 28. Macfarlan, T.S. *et al.* Embryonic stem cell potency fluctuates with endogenous retrovirus activity. *Nature* **487**, 57-63
859 (2012).
860 29. Wu, J. *et al.* The landscape of accessible chromatin in mammalian preimplantation embryos. *Nature* **534**, 652-657
861 (2016).
862 30. Zhu, Y. *et al.* Relaxed 3D genome conformation facilitates the pluripotent to totipotent-like state transition in
863 embryonic stem cells. *Nucleic acids research* **49**, 12167-12177 (2021).
864 31. Skene, P.J. & Henikoff, S. An efficient targeted nuclease strategy for high-resolution mapping of DNA binding sites.
865 *Elife* **6**, e21856 (2017).
866 32. Sasaki, F. *et al.* A high-affinity monoclonal antibody against the FLAG tag useful for G-protein-coupled receptor
867 study. *Analytical biochemistry* **425**, 157-165 (2012).
868 33. Markoulaki, S., Meissner, A. & Jaenisch, R. Somatic cell nuclear transfer and derivation of embryonic stem cells in
869 the mouse. *Methods* **45**, 101-114 (2008).
870 34. Ji, S. *et al.* OBOX regulates mouse zygotic genome activation and early development. *Nature* **620**, 1047-1053 (2023).
871 35. Rajkovic, A., Yan, C., Yan, W., Klysik, M. & Matzuk, M.M. Obox, a family of homeobox genes preferentially
872 expressed in germ cells. *Genomics* **79**, 711-717 (2002).
873 36. Ge, S.X. Exploratory bioinformatics investigation reveals importance of "junk" DNA in early embryo development.
874 *BMC genomics* **18**, 1-19 (2017).
875 37. Zhong, Y.-f. & Holland, P.W. The dynamics of vertebrate homeobox gene evolution: gain and loss of genes in mouse
876 and human lineages. *BMC evolutionary biology* **11**, 1-13 (2011).
877 38. Wilming, L.G., Boychenko, V. & Harrow, J.L. Comprehensive comparative homeobox gene annotation in human
878 and mouse. *Database* **2015**(2015).
879 39. Lee, H.-S. & Lee, K.-A. Characterization and functional analysis of Obox4 during oocyte maturation by RNA
880 interference. *Clinical and Experimental Reproductive Medicine* **34**, 293-303 (2007).
881 40. Lee, H.S. *et al.* Obox4 critically regulates cAMP-dependent meiotic arrest and MI-MII transition in oocytes. *The*
882 *FASEB Journal* **24**, 2314-2324 (2010).

41. Lee, K.-A., Lee, H.-S., Kim, E.-Y., Kim, K.-H. & Kim, Y. Oocyte-specific homeobox 4 (Obox4) is a key regulatory component of the cAMP-dependent meiotic arrest during in vitro oocyte maturation. *Fertility and Sterility* **90**, S108 (2008).
42. Lee, H.-S., Kim, E.-Y. & Lee, K.-A. Changes in gene expression associated with oocyte meiosis after Obox4 RNAi. *Clinical and experimental reproductive medicine* **38**, 68 (2011).
43. Lee, H.-S. *et al.* Obox4-silencing-activated STAT3 and MPF/MAPK signaling accelerate nuclear membrane breakdown in mouse oocytes. *Reproduction* **151**, 369-378 (2016).
44. Kim, H.-M. *et al.* Obox4 regulates the expression of histone family genes and promotes differentiation of mouse embryonic stem cells. *FEBS letters* **584**, 605-611 (2010).
45. Yang, L. *et al.* Transient Dux expression facilitates nuclear transfer and induced pluripotent stem cell reprogramming. *EMBO reports* **21**, e50054 (2020).
46. Leidenroth, A. & Hewitt, J.E. A family history of DUX4: phylogenetic analysis of DUXA, B, C and Duxbl reveals the ancestral DUX gene. *BMC evolutionary biology* **10**, 1-13 (2010).
47. Maeso, I. *et al.* Evolutionary origin and functional divergence of totipotent cell homeobox genes in eutherian mammals. *BMC biology* **14**, 1-14 (2016).
48. Zou, Z. *et al.* Translatome and transcriptome co-profiling reveals a role of TPRXs in human zygotic genome activation. *Science*, eabo7923 (2022).
49. Nowak, M.A., Boerlijst, M.C., Cooke, J. & Smith, J.M. Evolution of genetic redundancy. *Nature* **388**, 167-171 (1997).
50. Vavouri, T., Semple, J.I. & Lehner, B. Widespread conservation of genetic redundancy during a billion years of eukaryotic evolution. *Trends in genetics* **24**, 485-488 (2008).
51. Hackett, J.A. & Surani, M.A. Regulatory principles of pluripotency: from the ground state up. *Cell stem cell* **15**, 416-430 (2014).
52. Sakashita, A. *et al.* Endogenous retroviruses drive species-specific germline transcriptomes in mammals. *Nature structural & molecular biology* **27**, 967-977 (2020).
53. Bachtrog, D. Y-chromosome evolution: emerging insights into processes of Y-chromosome degeneration. *Nature Reviews Genetics* **14**, 113-124 (2013).
54. Zaret, K.S. Pioneer transcription factors initiating gene network changes. *Annual review of genetics* **54**, 367 (2020).
55. Eckersley-Maslin, M.A., Alda-Catalinas, C. & Reik, W. Dynamics of the epigenetic landscape during the maternal-to-zygotic transition. *Nature Reviews Molecular Cell Biology* **19**, 436-450 (2018).
56. Gassler, J. *et al.* Zygotic genome activation by the totipotency pioneer factor Nr5a2. *Science* **378**, 1305-1315 (2022).
57. Lai, F. *et al.* NR5A2 connects zygotic genome activation to the first lineage segregation in totipotent embryos. *Cell Research*, 1-15 (2023).
58. Grow, E.J. *et al.* p53 convergently activates Dux/DUX4 in embryonic stem cells and in facioscapulohumeral muscular dystrophy cell models. *Nature genetics* **53**, 1207-1220 (2021).
59. Sakashita, A. *et al.* Transcription of MERVL retrotransposons is required for preimplantation embryo development. *Nature genetics* **55**, 484-495 (2023).
60. Takeuchi, C., Murano, K., Ishikawa, M., Okano, H. & Iwasaki, Y.W. Generation of Stable Drosophila Ovarian Somatic Cell Lines Using the piggyBac System. in *piRNA: Methods and Protocols* 143-153 (Springer, 2022).
61. Guo, Y. *et al.* Potent mouse monoclonal antibodies that block SARS-CoV-2 infection. *Journal of Biological Chemistry* **296**(2021).
62. Sakurai, T., Watanabe, S., Kamiyoshi, A., Sato, M. & Shindo, T. A single blastocyst assay optimized for detecting CRISPR/Cas9 system-induced indel mutations in mice. *BMC biotechnology* **14**, 1-11 (2014).
63. Inoue, K. *et al.* Loss of H3K27me3 imprinting in the Sfmbt2 miRNA cluster causes enlargement of cloned mouse placentas. *Nature communications* **11**, 1-12 (2020).

927 64. Chen, S., Zhou, Y., Chen, Y. & Gu, J. fastp: an ultra-fast all-in-one FASTQ preprocessor. *Bioinformatics* **34**, i884-
928 i890 (2018).
929 65. Dobin, A. *et al.* STAR: ultrafast universal RNA-seq aligner. *Bioinformatics* **29**, 15-21 (2013).
930 66. Frankish, A. *et al.* GENCODE 2021. *Nucleic Acids Research* **49**, D916-D923 (2020).
931 67. Liao, Y., Smyth, G.K. & Shi, W. featureCounts: an efficient general purpose program for assigning sequence reads
932 to genomic features. *Bioinformatics* **30**, 923-930 (2014).
933 68. Hao, Y. *et al.* Integrated analysis of multimodal single-cell data. *Cell* (2021).
934 69. Zhong, Y.f. & Holland, P.W. HomeoDB2: functional expansion of a comparative homeobox gene database for
935 evolutionary developmental biology. *Evolution & development* **13**, 567-568 (2011).
936 70. Love, M.I., Huber, W. & Anders, S. Moderated estimation of fold change and dispersion for RNA-seq data with
937 DESeq2. *Genome biology* **15**, 1-21 (2014).
938 71. Langmead, B. & Salzberg, S.L. Fast gapped-read alignment with Bowtie 2. *Nature methods* **9**, 357-359 (2012).
939 72. Zhang, Y. *et al.* Model-based analysis of ChIP-Seq (MACS). *Genome biology* **9**, 1-9 (2008).
940 73. Ramírez, F. *et al.* deepTools2: a next generation web server for deep-sequencing data analysis. *Nucleic acids research*
941 **44**, W160-W165 (2016).
942 74. Yu, G., Wang, L.-G. & He, Q.-Y. ChIPseeker: an R/Bioconductor package for ChIP peak annotation, comparison
943 and visualization. *Bioinformatics* **31**, 2382-2383 (2015).
944 75. Bailey, T.L. *et al.* MEME SUITE: tools for motif discovery and searching. *Nucleic acids research* **37**, W202-W208 (2009).
945 76. Pohl, A. & Beato, M. bwtool: a tool for bigWig files. *Bioinformatics* **30**, 1618-1619 (2014).

946

Figure 1

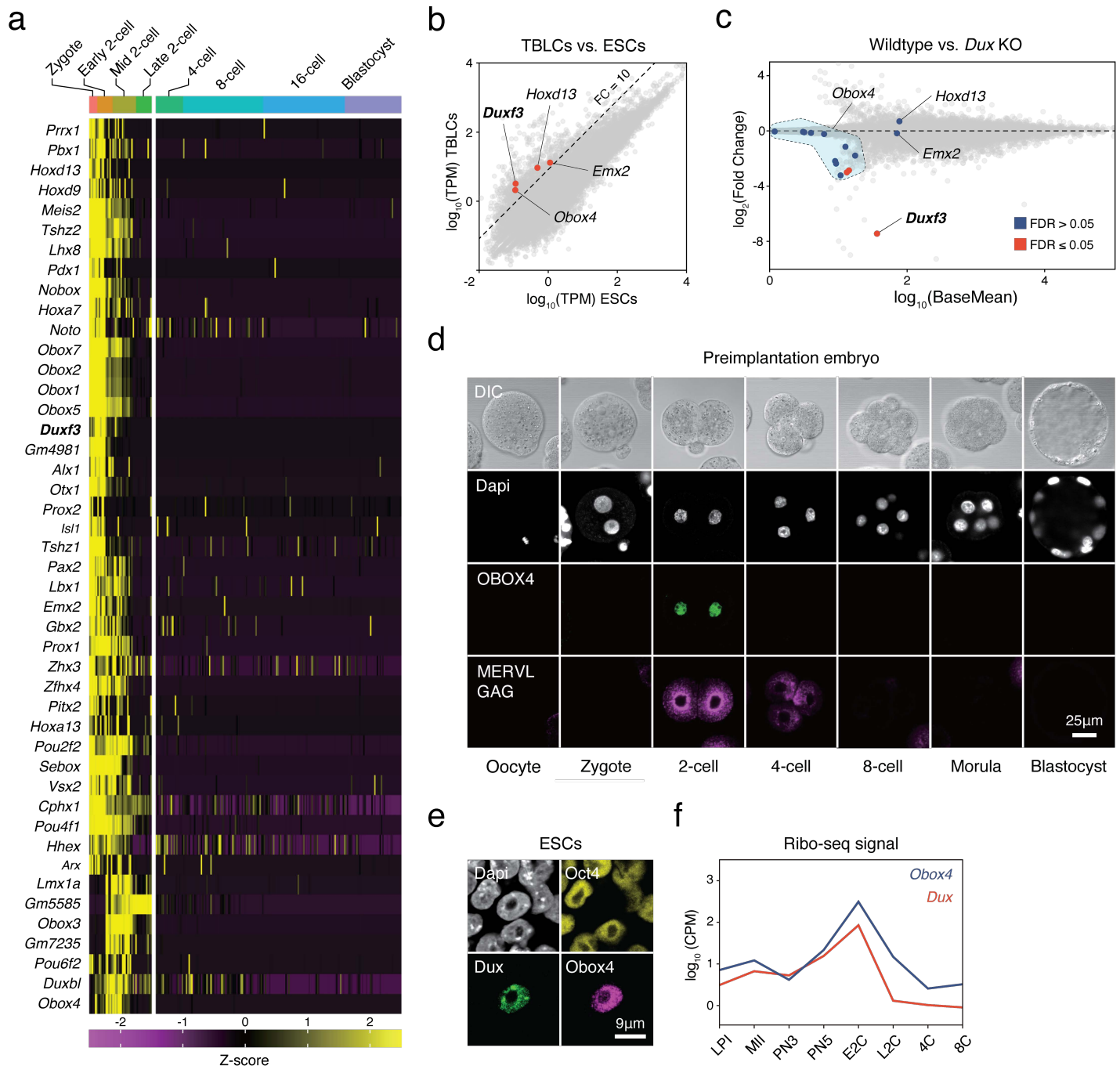
a
Zygote
Early 2-cell
Mid 2-cell
Late 2-cell
4-cell
8-cell
16-cell
Blastocyst
Prrx1
Pbx1
Hoxd13
Hoxd9
Meis2
Tshz2
Lhx8
Pdx1
Nobox
Hoxa7
Noto
Obox7
Obox2
Obox1
Obox5
Duxf3
Gm4981
Alx1
Otx1
Prox2
Isl1
Tshz1
Pax2
Lbx1
Emx2
Gbx2
Prox1
Zhx3
Zfhx4
Pitx2
Hoxa13
Pou2f2
Sebox
Vsx2
Cphx1
Pou4f1
Hhex
Arx
Lmx1a
Gm5585
Obox3
Gm7235
Pou6f2
Duxbl
Obox4
-2
-1
0
1
2
Z-score
b
TBLCs vs. ESCs
Hoxd13
Duxf3
FC = 10
Emx2
Obox4
log10(TPM) TBLCs
log10(TPM) ESCs
c
Wildtype vs. Dux KO
Obox4
Hoxd13
Emx2
Duxf3
FDR > 0.05
FDR ≤ 0.05
log2(Fold Change)
log10(BaseMean)
d
Preimplantation embryo
DIC
Dapi
OBOX4
MERVL GAG
25µm
Oocyte
Zygote
2-cell
4-cell
8-cell
Morula
Blastocyst
e
ESCs
Dapi
Oct4
Dux
Obox4
9µm
f
Ribo-seq signal
Obox4
Dux
log10 (CPM)
LPI
MII
PN3
PN5
E2C
L2C
4C
8C

Figure 2

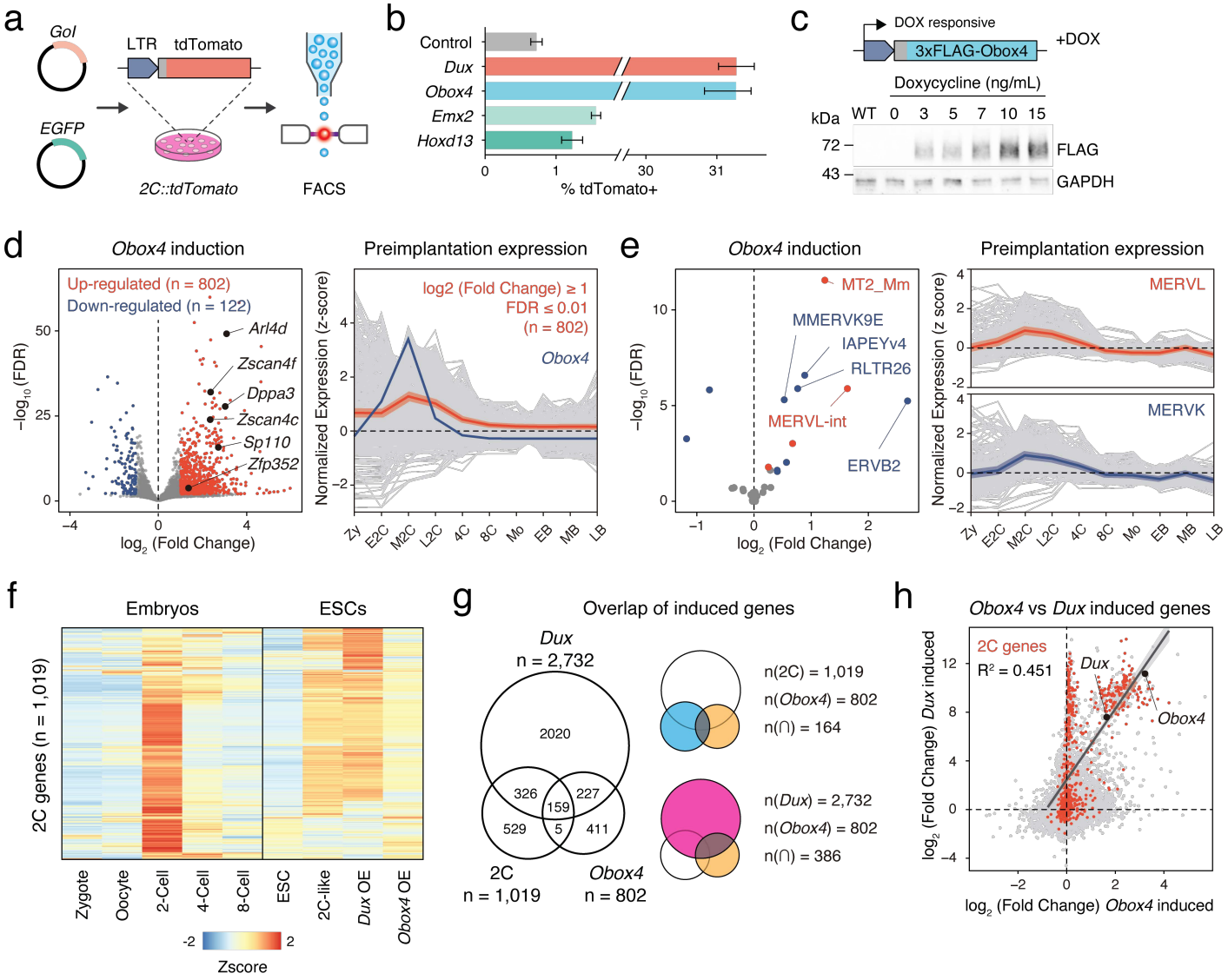
a
GoI
EGFP
LTR
tdTomato
2C::tdTomato
FACS
b
Control
Dux
Obox4
Emx2
Hoxd13
% tdTomato+
c
DOX responsive
3xFLAG-Obox4
+DOX
Doxycycline (ng/mL)
kDa
WT 0 3 5 7 10 15
72
43
FLAG
GAPDH
d
Obox4 induction
Up-regulated (n = 802)
Down-regulated (n = 122)
Arl4d
Zscan4f
Dppa3
Zscan4c
Sp110
Zfp352
−log10 (FDR)
log2 (Fold Change)
Preimplantation expression
log2 (Fold Change) ≥ 1
FDR ≤ 0.01
(n = 802)
Obox4
Normalized Expression (z-score)
Zy E2C M2C L2C 4C 8C Mo EB MB LB
e
Obox4 induction
MT2_Mm
MMERVK9E
IAPEYv4
RLTR26
MERVL-int
ERVB2
−log10 (FDR)
log2 (Fold Change)
Preimplantation expression
MERVL
MERVK
Normalized Expression (z score)
Zy E2C M2C L2C 4C 8C Mo EB MB LB
f
Embryos
ESCs
2C genes (n = 1,019)
Zygote
Oocyte
2-Cell
4-Cell
8-Cell
ESC
2C-like
Dux OE
Obox4 OE
-2
2
Zscore
g
Overlap of induced genes
Dux
n = 2,732
2020
326
227
159
529
5
411
2C
n = 1,019
Obox4
n = 802
n(2C) = 1,019
n(Obox4) = 802
n(∩) = 164
n(Dux) = 2,732
n(Obox4) = 802
n(∩) = 386
h
Obox4 vs Dux induced genes
2C genes
R² = 0.451
Dux
Obox4
log2 (Fold Change) Dux induced
log2 (Fold Change) Obox4 induced

Figure 3

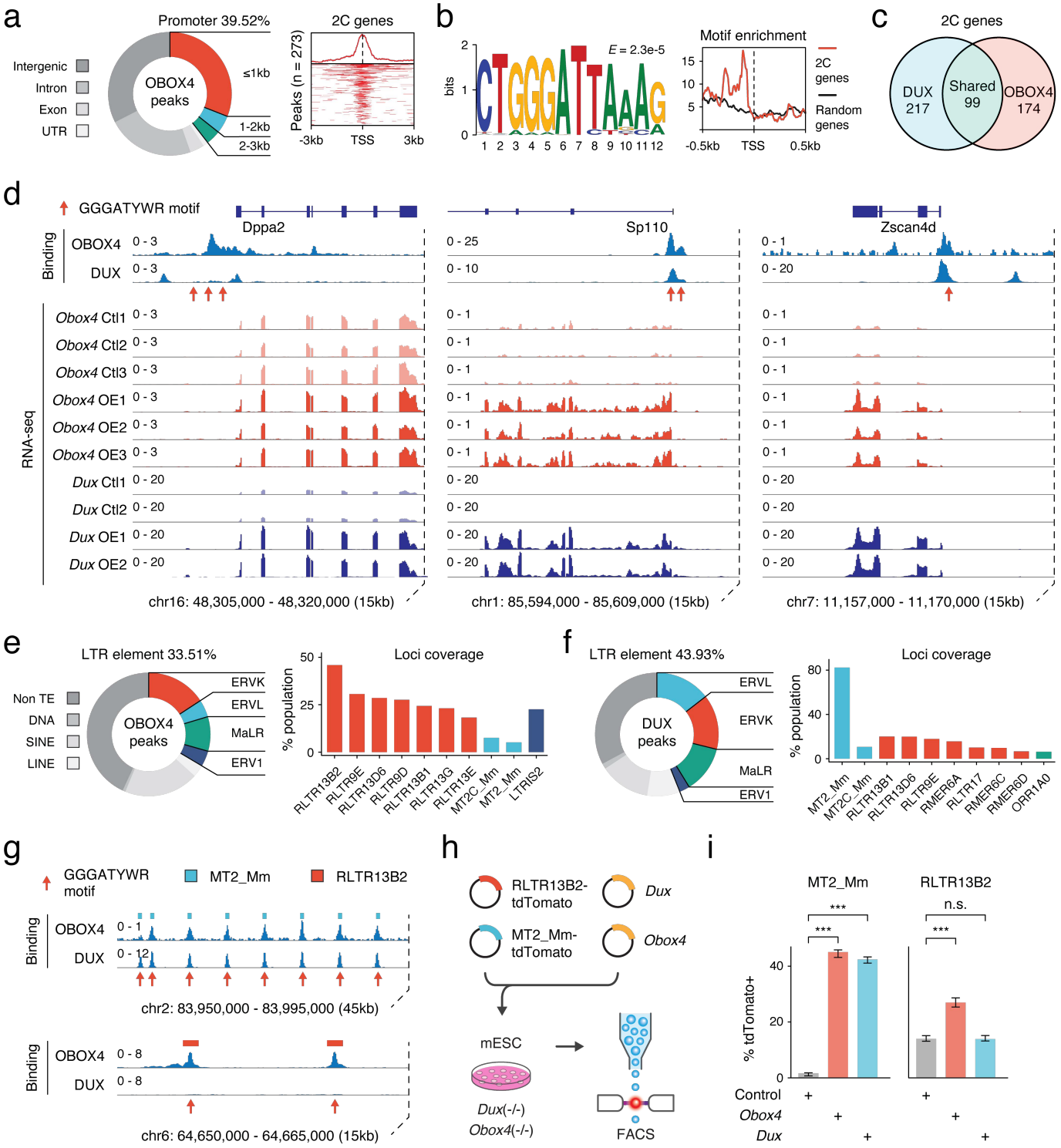
a
Promoter 39.52%
2C genes
Intergenic
Intron
Exon
UTR
OBOX4 peaks
≤1kb
1-2kb
2-3kb
Peaks (n = 273)
-3kb
TSS
3kb
b
E = 2.3e-5
bits
Motif enrichment
2C genes
Random genes
-0.5kb
TSS
0.5kb
c
2C genes
DUX 217
Shared 99
OBOX4 174
d
GGGATYWR motif
Dppa2
Sp110
Zscan4d
Binding
OBOX4
DUX
RNA-seq
Obox4 Ctl1
Obox4 Ctl2
Obox4 Ctl3
Obox4 OE1
Obox4 OE2
Obox4 OE3
Dux Ctl1
Dux Ctl2
Dux OE1
Dux OE2
chr16: 48,305,000 - 48,320,000 (15kb)
chr1: 85,594,000 - 85,609,000 (15kb)
chr7: 11,157,000 - 11,170,000 (15kb)
e
LTR element 33.51%
Non TE
DNA
SINE
LINE
OBOX4 peaks
ERVK
ERVL
MaLR
ERV1
Loci coverage
% population
RLTR13B2
RLTR9E
RLTR13D6
RLTR9D
RLTR13B1
RLTR13G
RLTR13E
MT2C_Mm
MT2_Mm
LTRIS2
f
LTR element 43.93%
DUX peaks
ERVL
ERVK
MaLR
ERV1
Loci coverage
% population
MT2_Mm
MT2C_Mm
RLTR13B1
RLTR13D6
RLTR9E
RMER6A
RLTR17
RMER6C
RMER6D
ORR1A0
g
GGGATYWR motif
MT2_Mm
RLTR13B2
Binding
OBOX4
DUX
chr2: 83,950,000 - 83,995,000 (45kb)
chr6: 64,650,000 - 64,665,000 (15kb)
h
RLTR13B2-tdTomato
Dux
MT2_Mm-tdTomato
Obox4
mESC
Dux(-/-)
Obox4(-/-)
FACS
i
MT2_Mm
RLTR13B2
n.s.
% tdTomato+
Control
Obox4
Dux

Figure 4

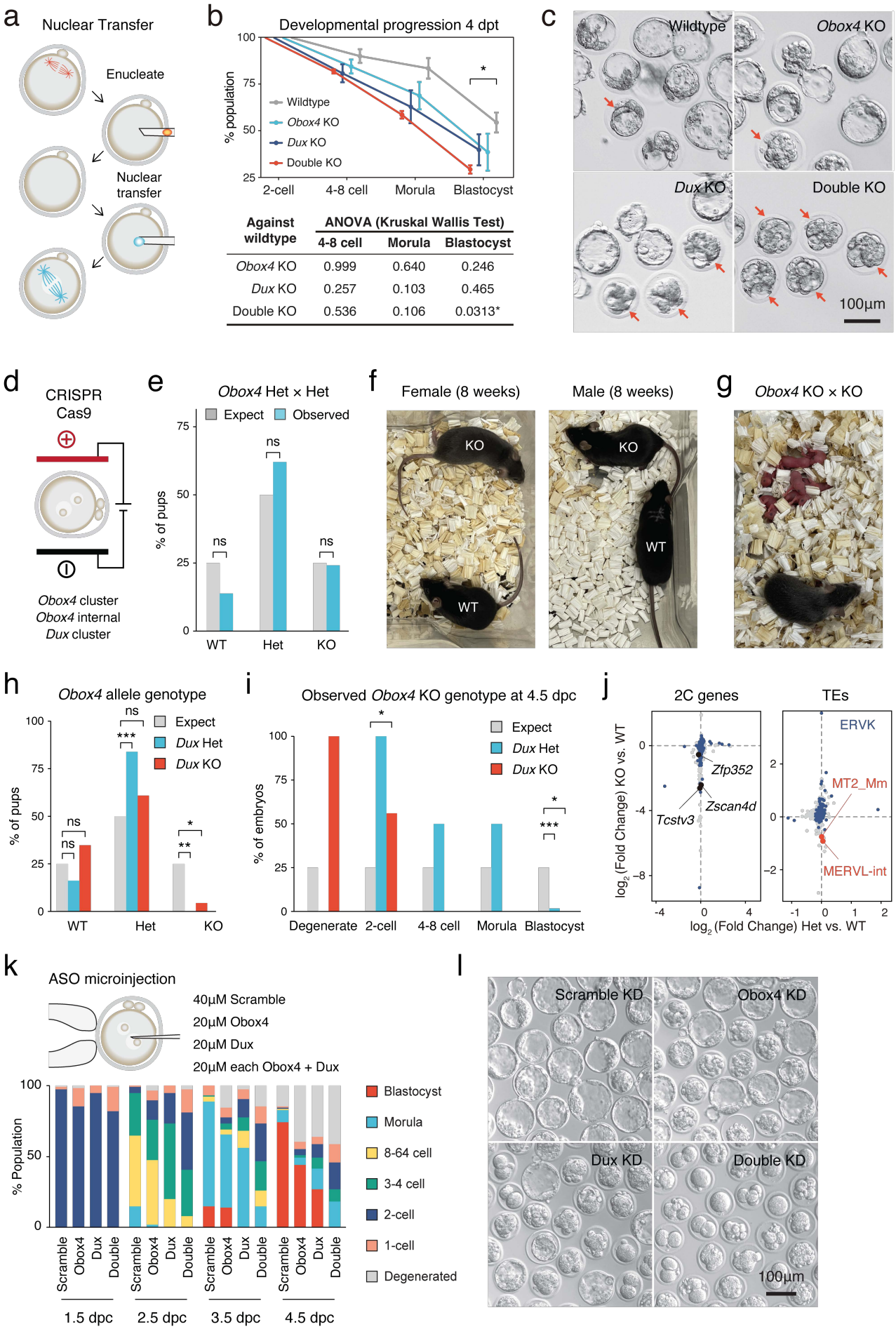

Against wildtype	ANOVA (Kruskal Wallis Test)		
	4-8 cell	Morula	Blastocyst
Obox4 KO	0.999	0.640	0.246
Dux KO	0.257	0.103	0.465
Double KO	0.536	0.106	0.0313*

Figure 5

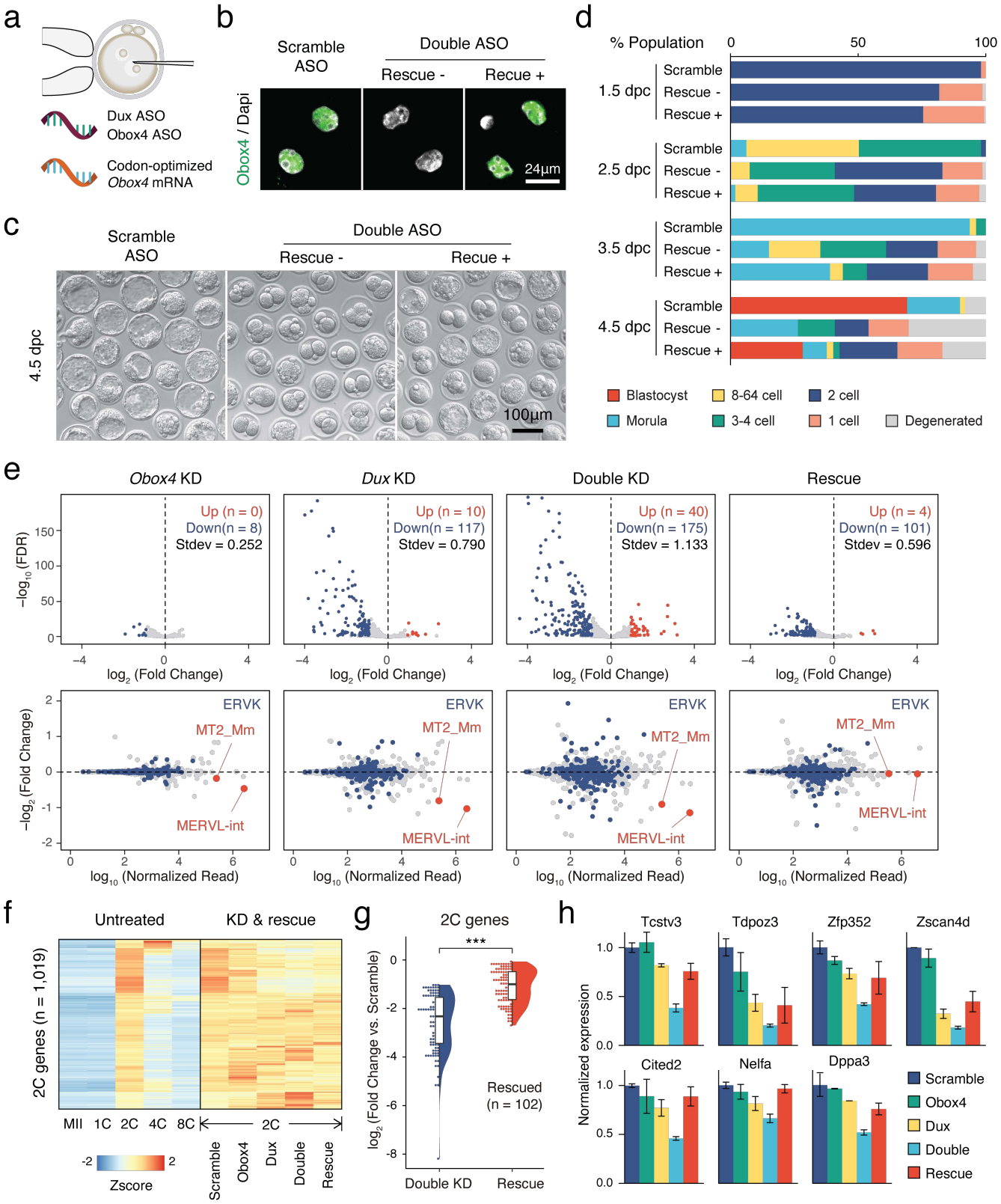
a
Dux ASO
Obox4 ASO
Codon-optimized
Obox4 mRNA
b
Scramble ASO
Double ASO
Rescue -
Recue +
Obox4 / Dapi
24µm
c
Scramble ASO
Double ASO
Rescue -
Recue +
4.5 dpc
100µm
d
% Population
0
50
100
1.5 dpc
2.5 dpc
3.5 dpc
4.5 dpc
Scramble
Rescue -
Rescue +
Blastocyst
8-64 cell
2 cell
Morula
3-4 cell
1 cell
Degenerated
e
Obox4 KD
Dux KD
Double KD
Rescue
Up (n = 0)
Down(n = 8)
Stdev = 0.252
Up (n = 10)
Down(n = 117)
Stdev = 0.790
Up (n = 40)
Down(n = 175)
Stdev = 1.133
Up (n = 4)
Down(n = 101)
Stdev = 0.596
−log10 (FDR)
log2 (Fold Change)
ERVK
MT2_Mm
MERVL-int
−log2 (Fold Change)
log10 (Normalized Read)
f
Untreated
KD & rescue
2C genes (n = 1,019)
MII
1C
2C
4C
8C
2C
Zscore
Scramble
Obox4
Dux
Double
Rescue
g
2C genes
***
log2 (Fold Change vs. Scramble)
Rescued
(n = 102)
Double KD
Rescue
h
Tcstv3
Tdpoz3
Zfp352
Zscan4d
Cited2
Nelfa
Dppa3
Normalized expression
Scramble
Obox4
Dux
Double
Rescue

Supplementary Figure 1

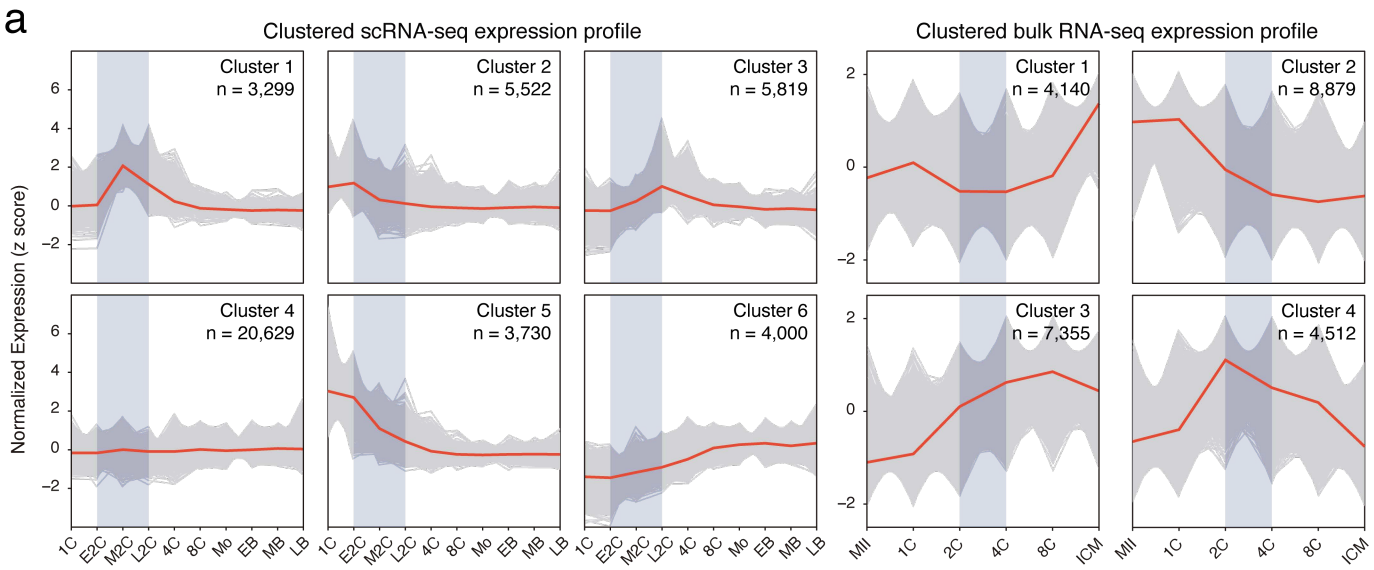

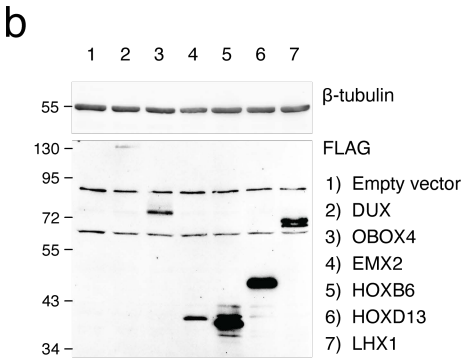

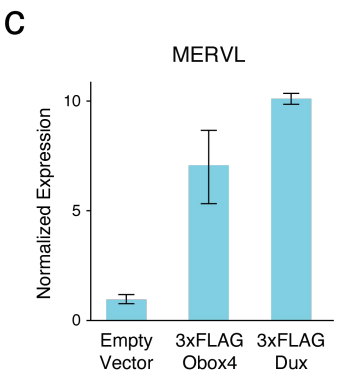

Supplementary Figure 2

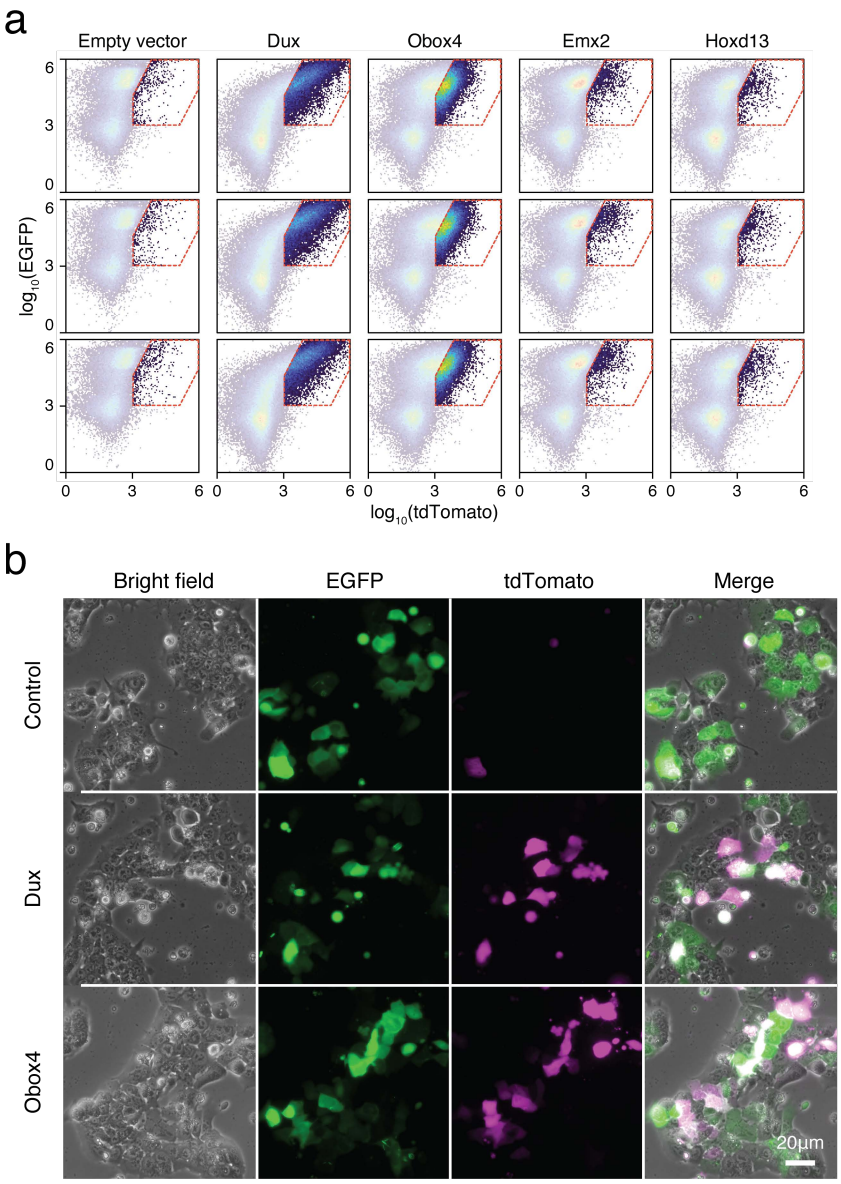

Supplementary Figure 3

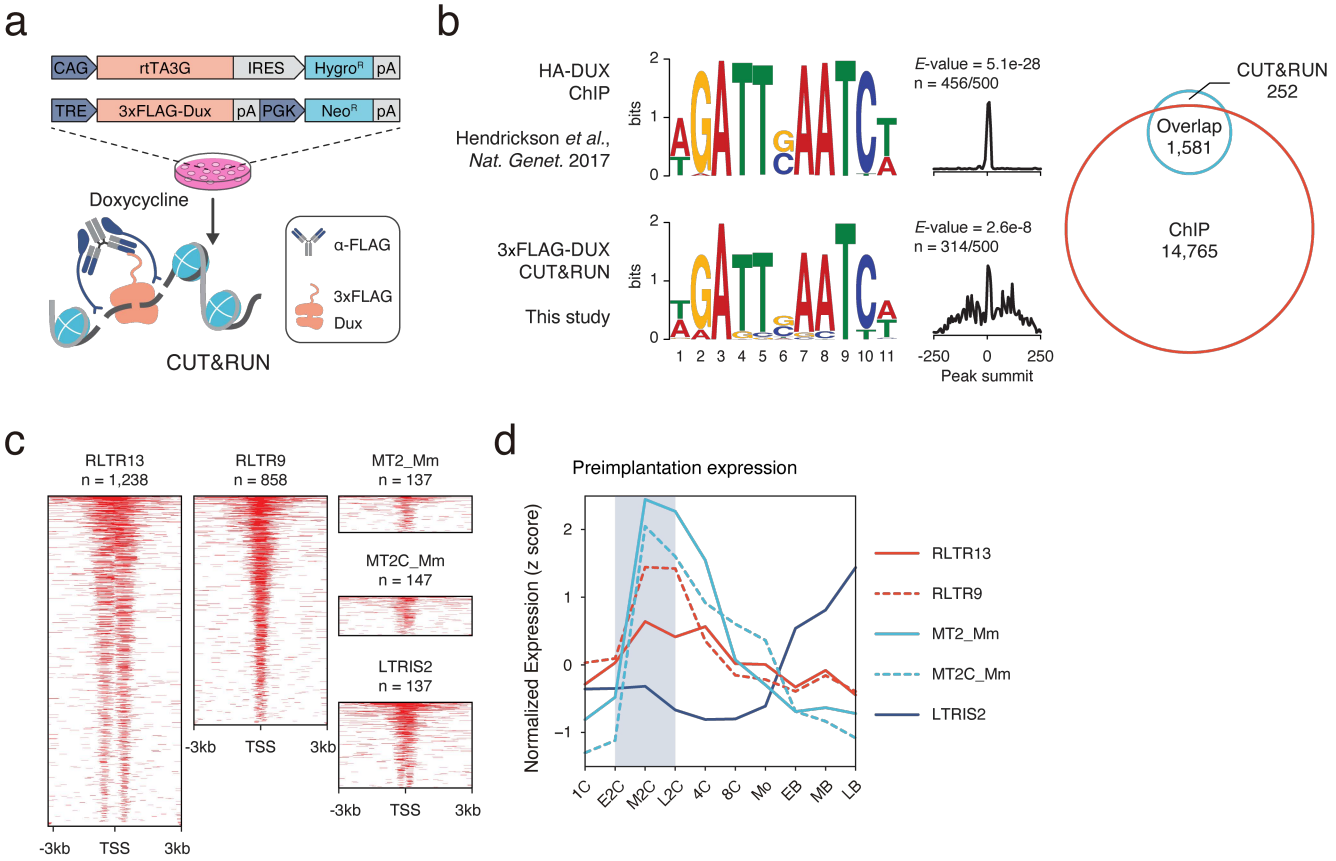

Supplementary Figure 4

Supplementary Figure 5

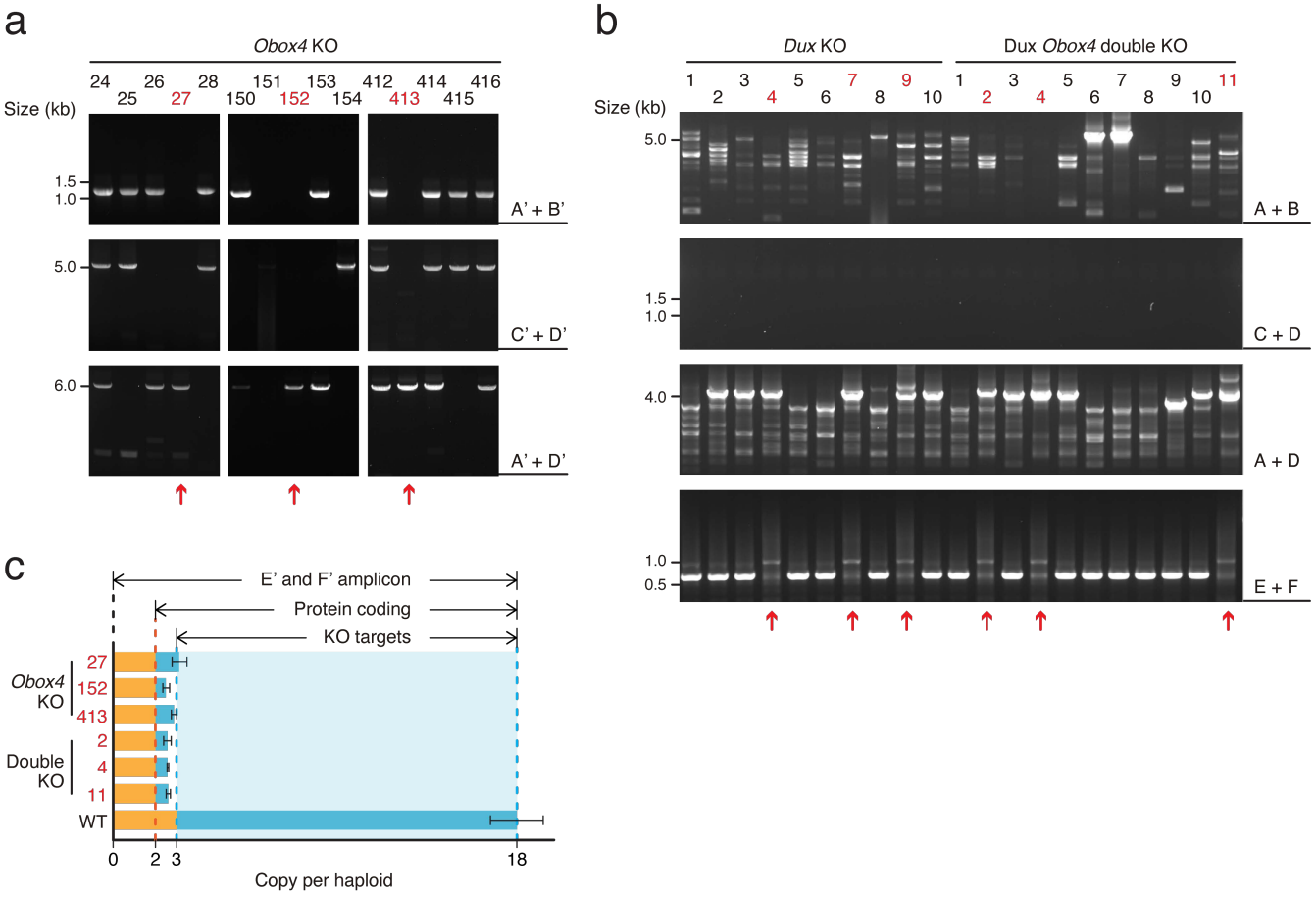

Supplementary Figure 6

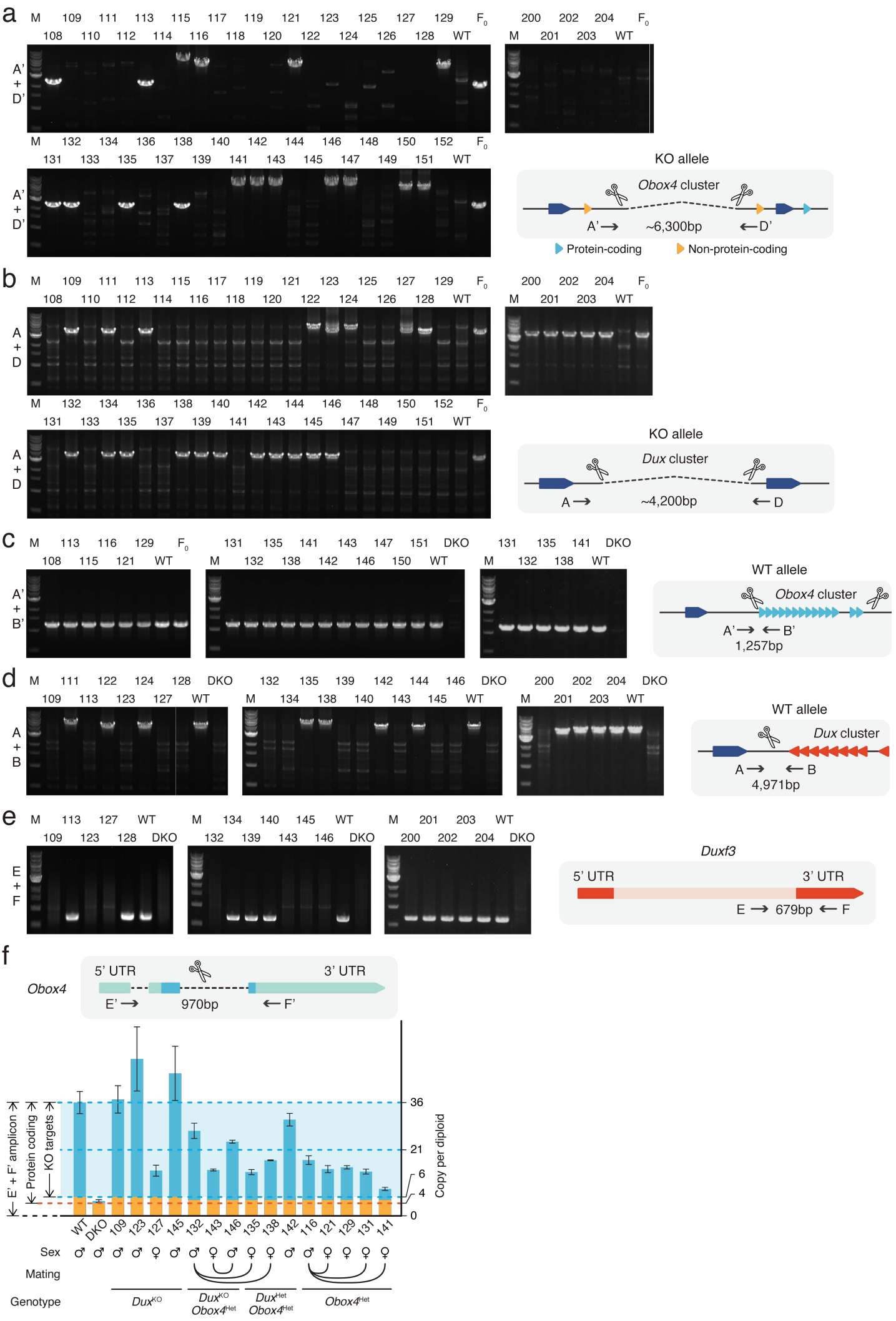

Supplementary Figure 7

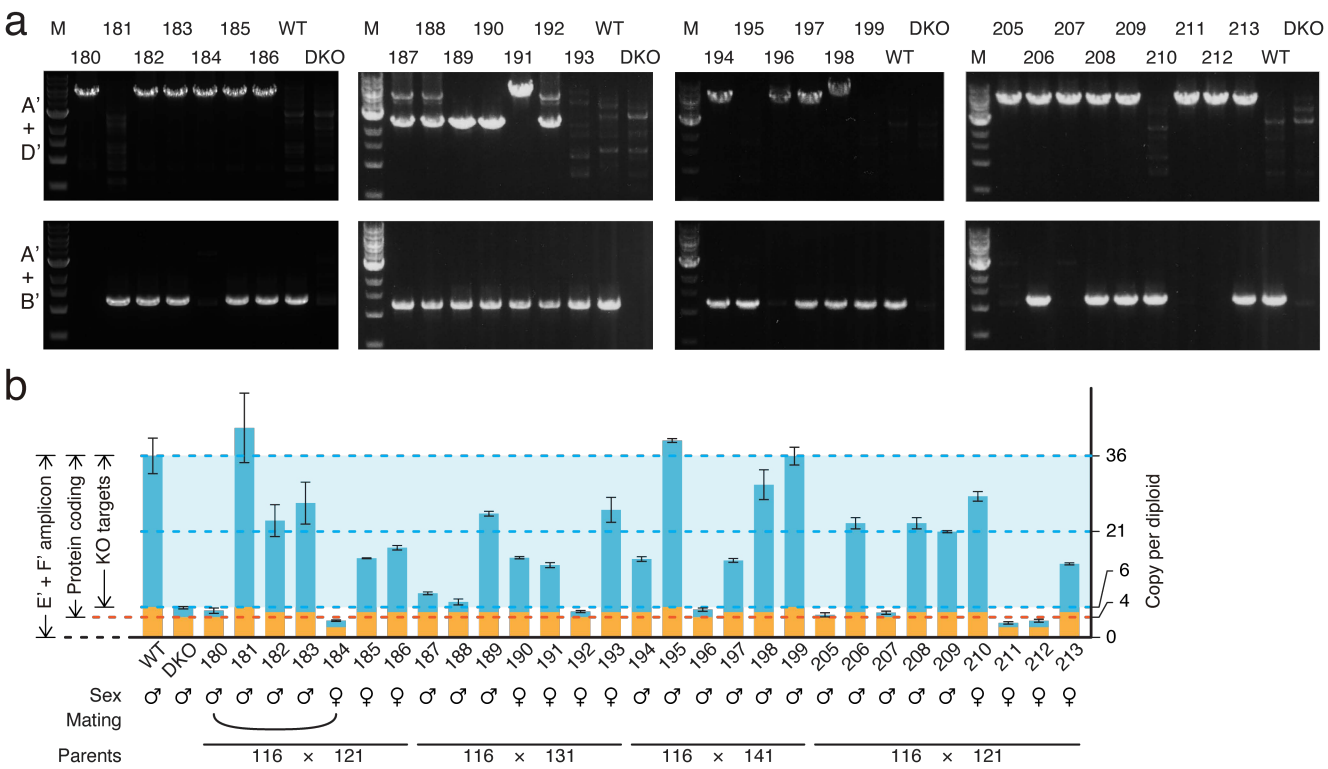

Supplementary Figure 8

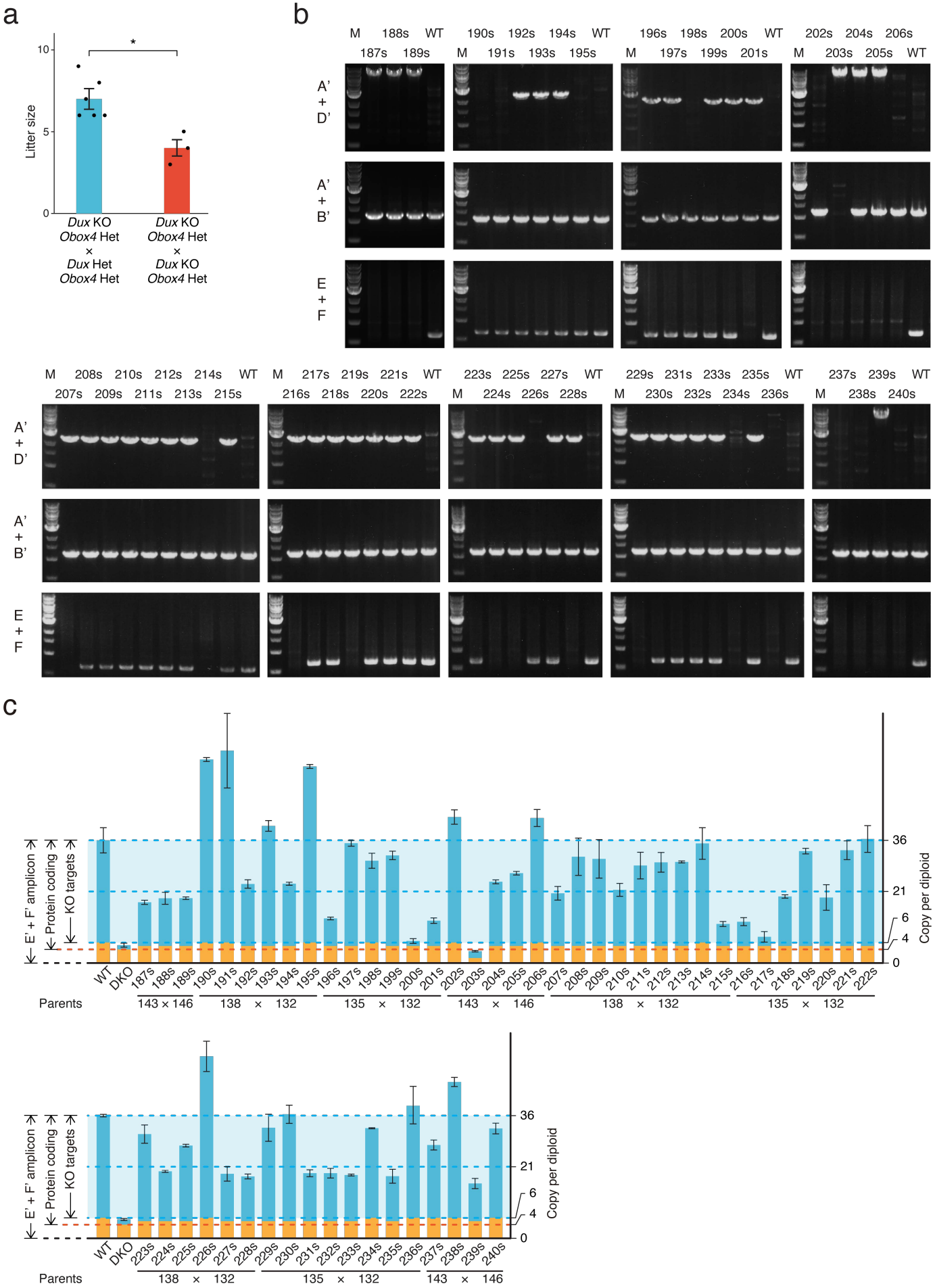

Supplementary Figure 9

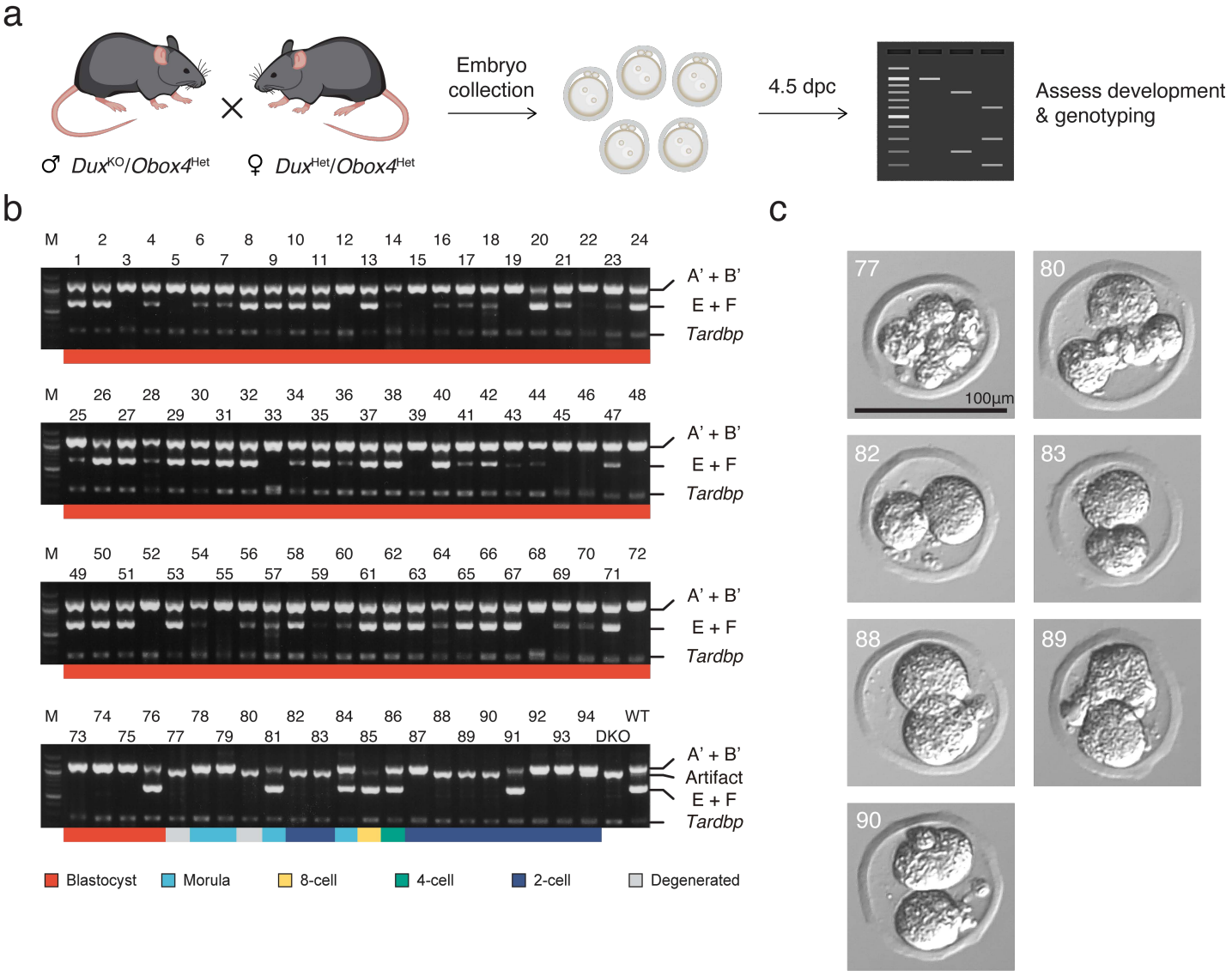

Supplementary Figure 10

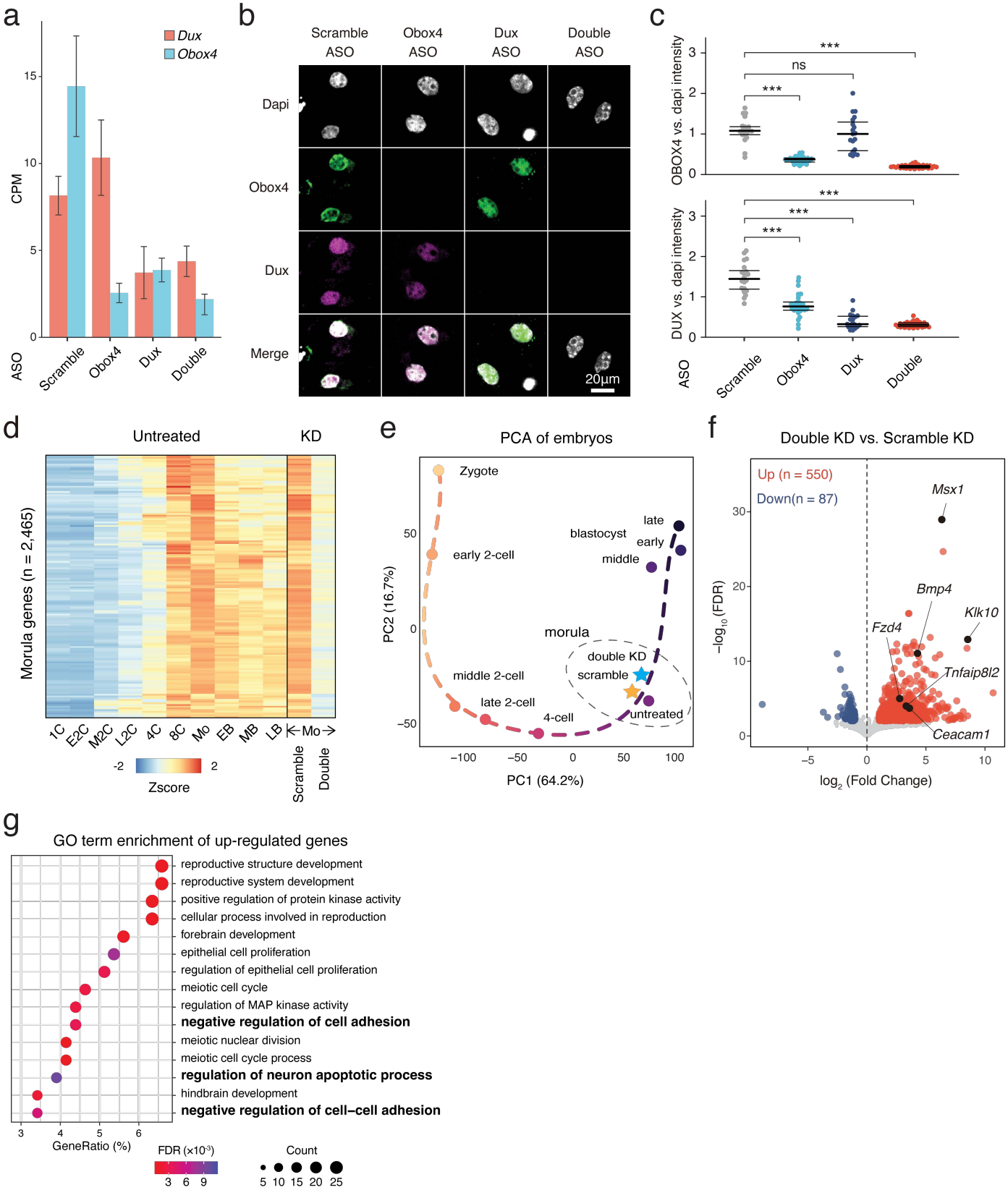
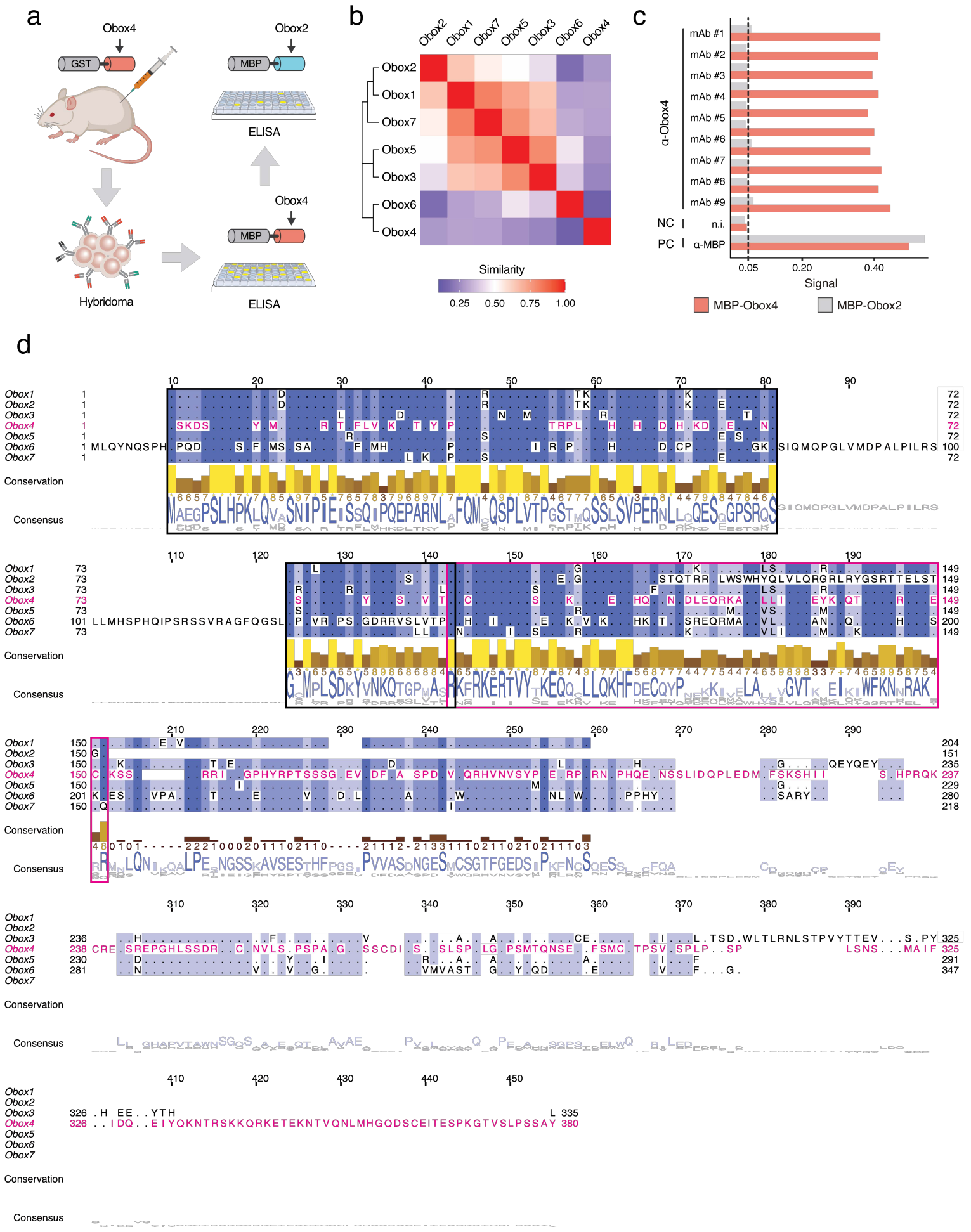
Supplementary Figure 11